Bohnhoff, M., Ickrath, M., Dresen, G. (2016): Seismicity distribution in conjunction with spatiotemporal variations of coseismic slip and postseismic creep along the combined 1999 Izmit-Düzce rupture. - *Tectonophysics*, *686*, pp. 132–145.

DOI: http://doi.org/10.1016/j.tecto.2016.07.029

Seismicity distribution in conjunction with spatiotemporal variations of coseismic slip and postseismic creep along the combined 1999 Izmit-Düzce rupture

Marco Bohnhoff[1,2, *], Michèle Ickrath[1], Georg Dresen[1]

(1) Helmholtz Centre Potsdam GFZ German Research Centre for Geosciences, Section 4.2: Geomechanics and Rheology, Telegrafenberg, Potsdam, Germany.

(2) Free University Berlin, Department of Earth Sciences, Malteser Strasse 74-100, 12249 Berlin, Germany.

* corresponding author (bohnhoff@gfz-potsdam.de)

Abstract

The North Anatolian Fault Zone (NAFZ) in NW Turkey as one of the most active and best studied strike-slip faults provides an unique opportunity to study earthquake related relaxation processes through analyzing co- and postseismic deformation. We study the spatial and temporal distribution of seismicity related to the two consecutive 1999 M>7 Izmit and Düzce earthquakes. A high-resolution aftershock catalogue including ~10,000 hypocenters extending along the combined rupture zone and extending from prior to the Izmit event to after the Düzce event is studied. Spatial and temporal distribution of events allow to identify distinct seismically active and inactive fault patches. Their location is related to the co- and postseismic deformation within and below the seismogenic layer, respectively. Four seismically inactive patches extending 30-50 kilometers along the rupture zone and down to 10 kilometers depth are identified with a systematic spatial shift between them introduced by the Dücze mainshock. The cumulative distribution of sub-areas hosting coseismic slip, aftershock clusters and postseismic creep shows that the entire upper (seismogenic) and lower (ductile) portion of the crust along the combined Izmit and Düzce rupture zone is activated between rupture initiation and a two-year postseismic period. This observation was only achieved due to the subsequent occurrence of two adjacent M>7 strike-slip earthquakes in combination with a distinct local seismic and geodetic monitoring. Our findings suggest that a coseismically introduced lateral and vertical slip deficit is systematically compensated postseismically in both the brittle and ductile portion of the crust.

Keywords

Seismotectonics, Seismicity, Spatial analysis; Seismic cycle; Earthquake dynamics; Seismicity and tectonics; NW Turkey, Postseismic Creep

1. Introduction

Studying co -and postseismic deformation is a key for the understanding of crustal relaxation processes that accompany and follow large earthquakes along continental transform faults. While coseismic deformation at the surface can be directly measured, the deformation processes at depth can only be deduced from inverting observations such as GPS-derived surface deformation, seismic waveforms, and extrapolated laboratory data. The fundamental challenge, however, is that the same postseismic surface deformation pattern can be produced by varying combinations of processes governing viscous shear and aseismic slip at depth (Burgmann and Dresen, 2008; Avouac, 2015). The investigation of co- and postseismic deformation has been improved by advances in geodetic techniques, such as the higher precision of GPS measurements and Interferometric Synthetic Aperture Radar (InSAR) range change data. For example high-resolution observations of time-dependent surface motions allow deriving improved transient deformation processes at depth (Burgmann and Dresen, 2008). First studies on the rheology at depth in conjunction with a major strike-slip earthquake were initiated by the great 1906 San Francisco earthquake on the San Andreas Fault. The analysis of surface deformation caused by this event first led to fundamental concepts of elastic rebound in the crust and the earthquake cycle (e.g. Reid, 1910; Thatcher, 1983). Throughout the last few decades, larger events along the San Andreas and adjacent faults provided the opportunity for extended in-depth studies. For the 1992 M_W7.4 Landers and 1999 M_W7.1 Hector Mine earthquakes in the Mojave Desert in California different possible mechanisms governing postseismic deformation such as deep aseismic afterslip, creep relaxation in the lower crust and upper mantle, a combination of poroelastic rebound and crustal afterslip or poroelastic rebound and creep relaxation in the lower crust and upper mantle were reported (see review by Burgmann and Dresen 2008, and references therein). In addition, for the Landers event, Perfettini and Avouac (2007) show that aftershocks and afterslip follow a similar temporal evolution and that the spatiotemporal distribution of aftershocks is consistent with the idea that they are driven by reloading of the seismogenic zone resulting from frictional afterslip.

Chang et al. (2013) used the transient postseismic geodetic signal measured at continuous GPS stations to model afterslip and frictional properties throughout the seismogenic crust after the 2004 Mw6.0 Parkfield earthquake. As for depth variations in afterslip Segall et al. (2000) for the Mw7.1 Loma Prieta earthquake and based on GPS data found that shallow afterslip dominated the postseismic deformation throughout the 8 years following the mainshock.

The complex interplay between coseismic dynamic rupture, aftershock seismicity throughout the brittle upper crust, frictional afterslip and other viscous flow mechanisms governing postseismic relaxation is still a matter of debate (e.g. Thatcher, 1983; Tse and Rice, 1986; Scholz, 2002; Perfettini & Avouac, 2004; Avouac, 2015). For example, considerable uncertainty in determining the hypocentral depth of local earthquakes along transform faults in absence of local seismic networks limits direct observation of the interaction between the brittle and ductile deformation in space and time related to major (M>7) strike slip earthquakes (e.g. Rolandone et al., 2004; Burgmann and Dresen, 2008). Rolandone et al. (2002) analyzed mechanical models of long-term deformation that suggest a wide zone of accommodated slip and ductile flow at the brittle-ductile transition and a change of the dominant deformation mechanisms during the earthquake cycle.

The aim of this study is to relate the spatiotemporal distribution of co- and postseismic brittle and ductile deformation throughout the entire crust along the combined rupture zone of the two adjacent 1999 Mw7.4 Izmit and Mw7.1 Düzce earthquakes in northwestern Turkey, two of the best-studied M>7 strike-slip earthquakes worldwide that occurred within 87 days (e.g., Tibi et al., 2001; Barka et al., 2002; Burgmann et al., 2002) (Fig. 1a). We determine and study the lateral- and depth distribution of aftershock seismicity from both events using data from local seismic networks deployed along the mainshock rupture zones (Fig. 1b). The data quality allows constraining aftershock activity along the rupture zones with unprecedented high precision. While the seismicity along the fault segments activated during the Izmit earthquake has been discussed earlier (e.g. Özalaybey et al., 2002; Bohnhoff et al., 2006; Bulut et al., 2007), here, an in-depth analysis also for the eastern portion of the combined Izmit-Düzce rupture including the Akyazi, Karadere and in particular the Düzce segments is provided for the first time. The aftershock pattern is then compared to the co- and postseismic deformation of both events.

We find that the Izmit and Düzce ruptures generate aftershock activity throughout the seismogenic layer of the crust leaving several 10 km deep and 30-50 km long aseismic patches that are considered to play an important role as barriers and asperities for future ruptures. Cumulative distribution of co- and postseismic brittle and ductile deformation and aftershock seismicity indicate that the entire crust is activated within a two-year period starting with the two consecutive M>7 ruptures.

2. Study area and database

The NAFZ is one of the largest plate-bounding transform faults, separating the Anatolian and Eurasian plates and extending for at least 1200 km between Eastern Anatolia and the Northern Aegean (e.g. Sengör et al., 2005; LePichon et al., 2015; Bohnhoff et al., 2016). Westward movement of Anatolia has developed in the framework of the northward moving Arabian plate and the southward rollback of the Hellenic subduction zone where the African lithosphere is subducted below the Aegean (Flerit et al., 2004; Bohnhoff et al., 2005; Bulut et al., 2012). The current right-lateral slip rate along the NAFZ is 20-30 mm/yr (e.g. Barka, 1992; McClusky et al., 2000; Reilinger et al., 2006), repeatedly producing major (M>7) strike-slip earthquakes of which the most recent ones were the Izmit and Düzce 1999 events that occurred in NW Turkey (Fig.1). Their combined rupture is ~200 km long connecting the Marmara segment of the fault in the west to the 1944 rupture in the east (Barka et al., 2002; Sengör et al., 2005; Bohnhoff et al., 2013).

2.1 Existing models for co- and postseismic deformation of the Izmit and Düzce earthquakes:

In order to study the relation between the seismicity along the combined Izmit and Düzce rupture presented in the following section and the co- and postseismic deformation of both events, we here briefly review available models of surface slip, coseismic slip and postseismic creep and compile averaged models (Figs. 2 and 3). Mapped and modeled right-lateral coseismic surface slip of the Aug17, 1999, Mw7.4 Izmit earthquake was reported by Barka et al. (2002) and Polat et al. (2002), both from field observations, Reilinger et al. (2000) and Tibi et al. (2001), both from GPS data, and Bos et al. (2004) from GPS and InSAR data. The different surface slip distributions are shown in Fig. 2a. The averaged and thus smoothed surface slip shows a ~100 km long surface rupture including a >15 km long maximum at the Sapanca segment reaching up to 5 m right-lateral slip while to either side about 2 m slip occurred. Towards the east, where the Düzce event occurred 87 days later the slip decreases gradually while the western end shows a sharp drop in slip. This is well explained by the rupture continuing westward offshore into the Sea of Marmara (where it is not mapped). Models for Izmit coseismic slip along the rupture and with depth were presented by Reilinger et al. (2000), Delouis et al. (2002) and Feigl et al. (2002) based on InSAR, GPS, teleseismic, SPOT measurements, and strong-motion data, respectively (Fig. 2b). The average coseismic slip model shows a ~70 km long and 15 km deep high-slip plane with >3 m slip including three local maxima where the slip was as high as 6 m at 5-10 km depth (Fig. 2b). The averaged model for post-seismic creep at depth (Fig. 2c) is based on reported data for the first 60–75 days following the Izmit earthquake obtained from inverting GPS data (Reilinger et al., 2000; Ergintav et al., 2009; Hearn et al., 2009) (Fig. 2c). Postseismic creep after the Izmit and prior to the Düzce event was modeled down to 40 km depth and shows two broader maxima below 15 km depth reaching 40 cm locally. Interestingly, a shallow patch with postseismic creep was observed slightly east of the Izmit epicenter (Fig 2c). We refer to this later in the text. Mapped and modeled right-lateral coseimic surface slip of the Nov12, 1999, Düzce Mw7.1 earthquake was reported by Akyüz et al. (2002) from field observations, Konca et al. (2010) correlating SPOT images, and Tibi et al. (2001) using GPS data (Fig. 3a). The average surface slip shows a rather symmetric bi-directional distribution with a maximum of ~4 m slowly decreasing to either side along a 40 km long surface rupture. The right-lateral coseismic slip distribution at depth indicates a 50-60 km long and ~20 km deep rupture plane with a local maximum of 2.5 m during the Düzce earthquake (Fig. 3b). The slip distribution was derived from averaging published results based on GPS and InSAR data (Burgmann et al., 2002), teleseismic and strong-motion data (Umutlu et al., 2004), and strong-motion and GPS data (Bouin et al., 2004) (Fig. 3b). Finally, we also compiled a postseismic (covering 1-2 years) creep model for the combined Izmit and Düze rupture. The postseismic creep distribution was derived from averaging inversion results from GPS data presented by Ergintav et al. (2009) and Hearn et al. (2009) and shows two major and a minor maximum extending down to 40 km locally reaching creep on the order of 30 cm/yr (Fig. 3c). A clearly non-uniform distribution of postseismic creep is observed within the seismogenic layer of the crust. This is further discussed in section 4.

2.2 A new hypocenter catalogue for the Izmit-Düzce region

To investigate the spatiotemporal distribution of seismically active and inactive fault patches along the Izmit and Düzce ruptures and their depth-extension as well as their relation to observed co- and postseismic slip at depth, an accurate hypocenter determination of the local seismicity is crucial. In this study we compiled a new hypocenter catalogue for the time period Jan 1997 (31 months prior to the Izmit earthquake) to Jan 2001 (14 months after the Düzce earthquake). This seismicity catalogue is mainly derived from seismic recordings of the SApanca-BOlu NETwork (SABONET) (Fig. 1b). SABONET consists of 15 stations equipped with Mark L4-3D 1Hz seismometers, 24-bit digitizers operated at a sampling rate of 100 Hz and global positioning system (GPS) timing (Milkereit et al., 2000; Baumbach et al., 2003; Bindi et al., 2007). SABONET was operated in event triggering mode during the time period considered here (1997-2001) except for the 2-month Izmit aftershock sequence when it was switched to continuous recording. Data processing steps and detailed characteristics of the SABONET hypocenter catalogue parameters containing 3,875 events (color-coded black in Fig. 4) are given in Ickrath et al. (2015). In addition to the catalogue we here enlarged the SABONET catalogue now including also smaller but well-recorded events (2,210 events, color-coded blue in Fig. 4). Waveforms of those events were manually picked and located using the HYPOCENTER location program (Lienert et al., 1986; Lienert and Havskov, 1995) based on HYPO71 (Lee and Lahr, 1972) using an optimized local 1D-velocity model from Bulut et al. (2007). The overall absolute hypocenter precision for all SABONET events is up to 3 km for 67% of the events. To improve the relative location accuracy, the events were relocated following the double-difference (hypoDD) earthquake relocation method by Waldhauser and Ellsworth (2000) leading to a relative location accuracy of approximately 500 m. In addition to the enlarged SABONET catalogue described above, the previously published Izmit aftershock catalogue of 3,833 relocated events with an internal precision of 400 m (Bulut et al., 2007) is also used (Fig.4, color-coded green). These events were located based on recordings from a temporarily denser network completed within 4 days after the Izmit mainshock (for details we refer to Bulut et al., 2007). No waveform recordings for the first two months following the Düzce earthquake were available to this study. The combined hypocenter catalogue for this study consists of a total of 9,918 events (Fig.4) and is freely available as an electronic supplement. The hypocentral distribution along the fault is plotted separately for the pre-seismic (before Izmit Aug 17, 1999), inter Izmit-Düzce (Aug 17 – Nov 11, 1999), and post-seismic (after Düzce Nov. 11, 1999) phase in figures 5 – 7 and discussed in the following section.

3. Results

The spatial distribution of seismicity along the two 1999 ruptures shows a clear variation in depth distribution and along the fault. The seismicity catalogue is plotted in map view and as depth section for three time intervals: prior to the Izmit earthquake, inter Izmit-Düzce and post-Düzce, respectively, in figures 5-7. In general, the seismicity is distributed along the entire combined rupture zone forming a ~20 km wide band of activity. This is consistent with previous studies that investigated the kinematic setting of the seismogenic zone from Izmit aftershocks (Aktar et al., 2004; Bulut et al., 2007; Bohnhoff et al., 2008; Görgün et al., 2009; 2010). In first-order approximation the activity level is increasing from west to east between 29.5°E and 31.5°E along the main rupture. The central part of the seismicity band does not exhibit a narrow vertical plane (the actual fault plane activated during the two mainshocks) which is not an artifact of hypocenter location precision. This observation is in accordance with Bouchon and Karabulut (2008) stating that a substantial portion of the Izmit aftershocks occurs off the main rupture, but not on the activated fault plane itself. Bouchon and Karabulut (2008) interpreted this as an additional constraint for the occurrence of super-shear rupture during the Izmit event. However, off-fault seismicity may also be related to fault zone maturity and roughness (Ben Zion and Sammis, 2003; Goebel et al., 2014a+b). The seismic activity along the Izmit rupture varies within individual fault segments consistent with the observed coseismic slip distribution and faulting kinematics (Barka et al., 2002; Özalaybey et al., 2002; Bohnhoff et al., 2006). In the following we discuss the combined Izmit and Düzce rupture zones for the three time periods separately relating the seismicity to co- and postseismic slip distribution:

3.1 Pre-Izmit time period:

For the pre-Izmit time period considered here (Jan 1997-Aug 16, 1999) the seismicity level is about two events/day and thus considerably lower than after the Izmit and Düzce mainshocks as expected. Most of the seismicity follows the main NAFZ fault branch with pronounced activity along the Izmit-Sapanca segment (see Fig. 5) that also hosted the Izmit hypocenter at its western part. In particular the area around the Izmit hypocenter has been recognized as a continuously seismically active patch during the years preceding the 1999 mainshock (Özalaybey et al., 2002; Aktar et al., 2004) and also showed immediate pre-shock activity preceding the Izmit mainshock (Bouchon et al., 2011). Apart from sparse seismicity that is distributed throughout the region, a pronounced seismicity cluster is observed at 30.4°E/40.9°N (Fig. 5). This activity most likely represents a quarry blast which is supported by the distribution of P-wave first-motion polarities (all positive) and from day-time occurrence of the events. We also note a second, less pronounced similar cluster at 31.2°E/41.1°N. Therefore, the seismicity within these two dense spatial clusters has been excluded from the depth section in figure 5 and from further analysis.

The main NAFZ fault branch east of 30.5°E is seismically inactive prior to the Izmit event except for a few individual events that are not clustered in space or time and likely represent background seismicity.

3.2 Inter Izmit-Düzce time period:

For the inter Izmit-Dücze time interval (Aug17-Nov11, 1999) a substantial increase in seismic activity and seismic moment release is observed concentrated on a ~20 km wide band along most of the Izmit rupture (Fig. 6). Note that the reduced seismic activity at the westernmost portion of the rupture below the eastern Sea of Marmara is due to the station distribution of the SABONET network (Fig. 1b). This part of the Izmit aftershock zone is not further analyzed here and has been studied e.g. by Özalaybey et al. (2002) and Bulut and Aktar (2007) based on recordings from local seismic stations.

The seismicity level is high for all fault segments activated during the Izmit mainshock, with significant lateral- and depth-dependent variations in hypocenter distribution. In particular, below the Lake Sapanca region and the Karadere Fault the upper boundary of aftershock activity extends as deep as 10 kilometers (marked A and B in Fig. 6b) while it is substantially shallower (<5 km) along the Akyazi and Düzce Basins both representing releasing bends separating strike-slip segments along the Izmit rupture (Bohnhoff et al., 2006; Görgün et al., 2010). The hypocenter depth variations between fault segments seem to correlate with the dominating faulting regimes. Segments with a normal faulting regime show seismicity reaching shallower (Ickrath et al., 2015) (Fig. 6b). Furthermore, the depth variation might also be related to structural variations along the fault since both areas with a 10-km deep aseismic zone are known to have a velocity contrast across the main fault (Bulut et al., 2012; Najdahmadi et al., 2016). Towards the eastern end of the Izmit aftershock activity zone there is a sharp termination of seismic activity at 31.2°E (Bulut et al., 2007; Bohnhoff et al., 2008). It was exactly on this edge where the Düzce earthquake nucleated 87 days following the Izmit event, on Nov. 11, 1999 (red star in Fig. 6b). The Düzce rupture then propagated mainly to the east while a small portion of the easternmost Izmit rupture plane was re-ruptured (Burgmann et al., 2002; Bouin et al., 2004; Umutlu et al., 2004; Konca et al., 2010) (Fig. 3b).

3.3 Post-Düzce time period:

For the post-Düzce time period (Jan 2000-Jan 2001), a clear shift in seismic activity towards the east is observed (Fig. 7). Most hypocenters are located at 5 to 15 km depth. Starting from the Sapanca segment in the west the density of events is substantially increasing. The highest level of seismic activity can be observed below the Akyazi, Karadere and Düzce segments of the fault zone. Interestingly, only about half of the earthquakes are located along the actual Düzce rupture. The other half primarily occurs on the same seismically active patches highlighted by Izmit aftershocks as during the Izmit aftershock phase 2.5 months prior to the Düzce event. Note that most of these patches showing pronounced aftershock seismicity after the Düzce event were not re-ruptured by the Düzce earthquake. The depth-distribution of seismicity shows a variation along the Düzce rupture with seismically less active shallow fault patches (marked as C and D in Fig. 7). However, below 10 km depth, aftershock activity is continuous along the rupture. While the depth resolution is uniform along most part of the Izmit-Düzce ruptures, the depth resolution for events along the easternmost Elmalik fault (east of ~31.2°E) is limited in response to the SABONET station distribution with only few stations to the east of the Düzce rupture (Figs. 1b and 7b).

Below the junction of the Karadere fault and the Düzce Basin (31°E, Fig. 7b) a cluster of high seismicity is observed with hypocenters distributed from < 3 km to 15 km depth. A similar seismic activity along this segment is also observed after the Izmit and prior to the Düzce event.

3.4 Shallow earthquakes on the Düzce fault:

While seismicity throughout the area and time period studied here is generally occurring within the depth interval 5-18 km there is a set of spatially isolated very shallow events located between 30.7-31.2°E and close to the activated main fault branch (red dots in Figs. 6b, 7b, 8). These 195 (~3 km shallow) events started to occur after the Izmit mainshock and are distributed along the junction of the Karadere and Düzce faults, within the seismically inactive patches B and C to a large extend (see Fig. 8 and discussion below). Therefore, their depth-constraint and internal spatiotemporal and kinematic pattern are of particular relevance. Since the depth is usually the least well constrained parameter of the hypocentral coordinates, the depth distribution of these events is further tested. For the 195 shallow events, the average rms error is 0.13 and on average 4 P picks and 3 S picks were used. S-P differential travel times provide a direct measure of the hypocentral distance from a seismic station. Values obtained at the two closest SABONET stations HEN and CND (see Fig. 1b for location) were analyzed and are shown in Fig. 9. The data show that the events are located at ~3 to 12 km distance from each station (for details we refer to Ickrath, 2015). This confirms that the 195 events are indeed very shallow and did not occur below ~3 km depth within the seismically inactive patches B and C. We refer to the role of these shallow events for the local kinematic setting later in the text.

3.5 Aseismic fault patches:

The here presented seismicity catalogue consists of ~10,000 events covering the time interval from ~2.5 years before the Izmit earthquake until 14 months after the Düzce earthquake. The most striking observation is that four distinct seismically inactive fault patches have been identified along the combined Izmit-Düzce rupture zone down to 10 km depth. Moreover, these four seismically inactive patches (labeled A-D in Figs. 6b and 7b) have different locations after the Izmit (before the Düzce) and after the Düzce mainshock. The spatial extent of these patches along the fault and with depth heavily depends on the depth-precision of the events in the surrounding area. The depth errors for all events are plotted in Fig. 8 suggesting that the aseismic behavior of all four patches A-D is well constrained. All four seismically inactive patches are described in detail in the following.

Patch A: For the inter Izmit-Düzce phase a nearly 50 km long seismically inactive patch extending down to ~10 km depth is observed east of the Izmit hypocenter along the Sakarya and Sapanca faults (Fig. 8a). Along the fault in the Izmit epicentral region and in particular the Akyazi plain, seismicity extends to shallower depths (4-5 km) limiting the inactive patch. Note that the seismically inactive fault patch is co-located with the largest maxima of the coseismic slip in the brittle crust (e.g., Reilinger et al., 2000) (Fig. 2b) and the cumulative 75-day afterslip below the seismogenic layer (e.g., Hearn et al. 2009) (Fig. 2c).

Patch B: Towards the East a second aseismic fault patch (B) is observed extending along the strike-slip Karadere fault extending ~10 km from the high-seismicity area in the pull-apart Akyazi Plain towards the western end of the Düzce basin and fault. Again, no seismicity is observed in this region down to ~10 km depth (Fig. 6b and 8). This zone contains several of the shallow earthquakes introduced earlier. Similar to patch A, a postseismic slip maximum was observed below this seismically inactive patch (e.g., Hearn et al. 2009) (Fig. 2c) for the inter Izmit-Düzce period of ~75 days. However, no direct correlation to the local coseismic slip maximum can be identified (Fig. 2b). It is noted, that patch B is located close to the eastern boundary of the Izmit rupture.

Patch C: For the postseismic phase after the Düzce event a clear spatial shift of shallow (but >3 km deep) seismicity clusters and seismically inactive fault patches is observed (Fig. 7 and 8). Patch C is similar in shape to patch A with regard to along-fault extension and depth. However, it is shifted by about 50 km to the east, into an area that hosted the overall strongest Izmit aftershock activity (below the Akyazi Plain). As for patches A and B for the inter Izmit-Düzce time period, regions C and D are just above the maxima in postseismic slip (one year time period) found below the seismogenic layer (e.g., Hearn et al. 2009) (Fig. 3c). No coseismic slip during the Düzce event was observed at the location of patch C, probably because this fault portion had already coseismic deformation during the Izmit event and thus shear stress was still low at the time of the Düzce event (only 87 days later).

Patch D: The seismically inactive patch D is located further to the east below the Düzce Basin reflecting a releasing bend and extends 40 km along the main fault branch of the NAFZ activated during the Düzce event (Figs. 7 and 8). Similar to the other three seismically inactive patches A-C also D extends down to 10 km depth and is underlain by a maximum in Düzce-postseismic deformation below the seismogenic layer. Different to the patches A-C this patch coincides with the coseismic slip maximum area of the Düzce earthquake to a large extent covering the eastern half of the Dücze high-slip area.

4. Discussion

The seismicity catalogue presented here consists of ~10,000 events extending along the entire combined Izmit-Düzce rupture zone. In total, the Izmit and Düzce mainshocks ruptured an almost 200 km long part of the NAFZ in northwestern Turkey extending from the eastern Sea of Marmara in the west to the western end of the 1944 rupture in the east (e.g. Tibi et al., 2001; Barka et al., 2002). This is the first hypocenter catalogue obtained from a local seismic network for the time period extending from ~2.5 years prior to the Izmit to 14 months after the Düzce event. The catalogue includes reliable hypocenters with a precision of up to 3 km in lateral and vertical directions.

During the two years prior to the two consecutive 1999 Izmit and Düzce M>7 mainshocks, sparse seismic activity is observed throughout the area with some spatial clustering along distinct parts of the main branch of the NAFZ (Fig. 5). Hypocentral depths are mostly between 10 and 18 km, i.e. most of the seismicity is located in the lower part of the seismogenic layer. Following the Izmit and Düzce mainshocks the overall seismicity rate drastically increased (Figs. 6 and 7). The spatiotemporal distribution of events allows defining several interesting features:

In map view the seismicity forms an approximately 20 km wide band of activity with most events concentrated along the main fault trace. This broad off-fault damage zone was activated during the 1999 M_W 7.4 Izmit and M_W 7.1 Düzce earthquakes (Fig. 6 and 7). The off-fault location of seismicity, as observed also before the Izmit and after the Düzce events, is in good correspondence with previous observations covering the initial two-month Izmit aftershock period (Bulut et al., 2007; Bohnhoff et al., 2008; Görgün et al., 2010). It is also in agreement with other Izmit aftershock observations that were interpreted to be indicative of super-shear rupture during the Izmit event (Bouchon & Karabulut, 2008). The seismicity distribution off the fault likely characterizes the width of the damage zone surrounding the principal slip zone of the rupture (Ben Zion and Sammis, 2003; Goebel et al., 2014a+b). Small secondary faults may have been activated during dynamic rupture along the principal slip zone.

We observe a relatively sharp lower boundary of seismicity throughout the whole study area, i.e. along the combined Izmit-Düzce ruptures. Within the 3 km uncertainty in depth resolution this lower boundary is consistently located at about 18 km depth. Below this depth fault slip along the

NAFZ is stable and deformation may be increasingly accommodated by semi-brittle and plastic flow mechanisms. Rolandone et al. (2004) studied variations in maximum depth of seismicity during the years following the Landers earthquake in California. The authors analyzed the evolution of the lower hypocentral depth for aftershocks and found a time-dependent postseismic shallowing of about 3 km within a time span of 4 years following the Landers earthquake. Within the more limited time period investigated here, we do not find any significant depth changes in seismicity.

Our hypocenter catalogue highlights significant changes in seismicity in space and time along the different fault segments of the NAFZ. Fault segmentation was observed both coseismically in terms of rupture propagation and slip distribution (Tibi et al., 2001; Gülen et al., 2002; Barka et al., 2002) as well as from studying aftershock focal mechanisms (Bohnhoff et al., 2006; Ickrath et al., 2014; 2015). The most prominent aftershock activity occurs along the Akyazi Plain that represents a local pull-apart structure hosting a >3 m along-strike slip deficit introduced by lateral variations of coseismic slip along the Izmit rupture (e.g. Barka et al. 2002; Aydin and Kalafat 2002). The complex fault structure and the rupture process caused significant coseismic changes in local stress orientation at the fault along the Akyazi fault segment within the first weeks following the Izmit mainshock (Bohnhoff et al., 2006; Ickrath et al., 2014; 2015). Moreover, significant isotropic non-double-couple components in the seismic moment tensors were observed in that area decreasing within the first two months following the Izmit mainshock (Stierle et al., 2014a+b). The coseismically introduced strike-slip deficit at this fault segment may have been in part compensated by prolonged postseismic normal-faulting distributed in the Akyazi pull-apart structure.

It is noted that the Düzce mainshock drastically disturbed the Omori-type decline of aftershock activity along the Izmit rupture. The event completely reorganized the spatial occurrence of local seismicity during the time period 2-14 months following the Düzce event (Fig.7). The spatial distribution shows a remarkable eastward shift of the seismicity in response to the eastward extension of the rupture introduced by the Düzce mainshock. Similar to the distribution of Izmit aftershocks, the post-Düzce seismicity shows clear lateral variations in seismic activity along the rupture. In particular, it is noted that the depth distribution of seismicity below the Akyazi plain changed after the Düzce mainshock. Shallow (<10 km) seismicity was 'switched off' while deeper events continued to occur (Fig. 8). In contrast, shallower seismicity in between the Akyazi Plain and the Düzce basin including the Karadere fault was 'switched on' by the Düzce mainshock.

The striking feature from this new hypocenter catalogue is that seismic activity along the Izmit-Düzce rupture reveals strong lateral changes defining clearly delimited inactive patches extending from the surface down to 10 km depth, i.e. covering the upper ~60% of the seismogenic layer. We observe four patches (labeled A-D in Figs. 6b and 7b) that extend between 10 and 50 km in length along the main fault branch activated during the Izmit and Düzce mainshocks, respectively. The position of these patches varies laterally between time periods separated by the Izmit and Dücze mainshocks.

The co- and postseismic stress changes due to the Izmit and Düzce earthquake have been studied in kinematic models using the inferred coseismic fault slip for both earthquakes (e.g. Reilinger et al., 2000; Delouis et al., 2002; Hearn et al., 2009) as summarized in section 2. In Figure 2 and 3 the average distribution of surface-, co-, and postseismic slip is indicated separately for the Izmit and Düzce events, respectively. There, the postseismic periods extend over 75-days (inter Izmit-Düzce) and 2 years (postseismic Düzce) following the mainshocks.

Two spatially separated doublets of aseismic fault patches were observed during the inter Izmit-Düzce and post-Düzce phase, respectively. Analyzing the occurrence of seismically inactive fault patches, a clear co-location with the maximum in postseismic deformation below the seismogenic layer in the lower crust is found. In the following these four patches are discussed in relation to the local seismotectonic setting, and the coseismic and postseismic slip distributions.

Patches A-D and their local seismotectonic context: The patches A (Sapanca) and B (Karadere) are located in areas where the local NAFZ fault branch is mostly a vertical strike-slip fault, although fault trends differ (EW in the Sapanca area, N65°E along the Karadere fault). Moreover, both patches are located along NAFZ segments with a known velocity contrast across the fault at crustal depth (Sapanca ~6%, Karadere ~4%) (Bulut et al., 2012; Najdahmadi et al., 2016). The two patches are separated by the Akyazi Plain as a pull-apart basin. The patches C (Akyazi Plain and western Karadere fault) and D (Düzce fault) also include vertical or steeply inclined strike-slip faults. However, in contrast to patches A and B they are co-located with the Akyazi and Düzce pull-apart basins. This suggests that there is a relation between fault segmentation and patches geometry. A possible explanation for a common characteristic of all four patches might be, that the stress drop of the two mainshocks on the principal slip zones relaxed these vertical strike-slip faults (principal slip zones) with the result that they hosted no shallow aftershocks. The aftershocks then mainly occurred along portions of the seismogenic crust facing a coseismically introduced lateral or vertical slip deficit.

<u>Patches A-D and coseismic slip distribution:</u> The Izmit event and to some extent also the Düzce event are among the best studied M>7 earthquakes. This also holds for the along-fault distribution of coseismic slip that has been studied in detail (e.g. Reilinger et al., 2000; Delouis et al., 2002) and summarized in section 2. The Izmit event had an average right-lateral slip of ~2.3 m, but in part strong lateral and vertical variations were observed along the rupture (e.g., Gülen et al., 2002). The main high-slip patch with slip maxima on the order of 6 m was identified along a ~80 km long segment including the Izmit hypocenter. A second high-slip patch representing the last interval of the rupture was located at the eastern end of the rupture (Fig. 2a). The Düzce event reflects a rather bi-directional symmetric slip distribution of up to 2.5 m extending to either side of the hypocenter along a ~60 km long fault segment coinciding with the Düzce fault to a large extent. While patch A covers approximately half of the western main high-slip patch of the Izmit earthquake (the other half hosting numerous shallow aftershocks), patch B is located in area of low to intermediate coseismic slip but close to the high-slip patch at the eastern end of the rupture. Patch C is located in an area where almost no coseismic slip occurred during the Düzce event, while patch D covers most of the high-slip area of the Düzce event. In summary no simple systematic relation between coseismic slip maximum and the four patches A-D extending throughout the upper half of the seismogenic layer is observed.

Patches A-D and postseismic slip distribution: Interestingly, the along-fault extension of deep postseismic slip shows a large overlap with the seismically inactive patches below the seismogenic zone at a depth of 30-40 km for the inter Izmit-Düzce time period (patches A, B) (60-75 days) and for the period after the Dücze event (patches C, D) (1-2 years). The slip distribution reveals two postseismic slip maxima each for both time periods indicating a heterogeneous slip distribution along strike similar to the heterogeneous aftershock activity observed in the upper crust. It is conceivable that postseismic slip is accommodated by stable frictional afterslip and brittle creep (Perfettini & Avouac, 2004). However, at elevated temperatures and pressures at greater depth crystal plastic deformation and/or solution precipitation creep may also contribute to postseismic slip.

No first-order postseismic creep was observed at seismogenic depth except for one isolated shallow spot at the central Sapanca segment after the Izmit event (Fig. 2c) (after Reilinger et al., 2001; Ergintav et al., 2009; Hearn et al., 2009) and one spot following the Düzce event and located around the Izmit epicenter that is connected to the overall postseismic creep maximum extending down to >35 km depth (Fig. 3c) (Ergintav et al., 2009; Hearn et al., 2009) . Hearn et al. (2002) assumed that the early postseismic phase of the Izmit earthquake is dominated by localized velocity-strengthening afterslip on the downdip extension of the coseismic rupture rather than with distributed viscous flow in the lower crust or upper mantle. However, taking into account the different models of frictional afterslip, kinematic slip inversion and viscous shear zones by Hearn et al. (2009) they assume that the deformation processes on a longer time scale suggest additional contributions of viscous flow in the lower crust and/or upper mantle.

Pucci et al. (2006; 2007) modeled slip distribution at depth obtained by different joint inversions of teleseismic, strong motion, GPS and InSAR data (e.g. Bürgmann et al. 2002; Çakir et al. 2003a). Similar to the observed aseismic patch D in figure 5b and based on the resulting slip distribution at depth, Pucci et al. (2007) observe a single, round-shaped, 10-25 km-wide, 6-8 meters slip maximum located in the eastern part of the Düzce fault. Generally these authors and others (Cakir et al., 2003b; Ergintav et al., 2009) concluded that the earliest Izmit postseismic deformation was dominated by rapid afterslip at seismogenic depths followed by an extremely rapid decay of the postseismic transient component (Bürgmann et al., 2002; Hearn et al., 2002; 2009). Following early afterslip in the upper brittle part of the crust, slip was progressively transferred to deeper parts of the crust. Postseismic slip partly compensates a slip deficit that occurred in deeper parts of the crust compared to an average coseismic displacement of 2.3 m. Two inter Izmit-Düzce postseismic slip maxima extend for about 40-50 km along the fault (Fig. 2c). The two slip maxima show a clear co-location with the seismically inactive patches A and B (Fig.10). Spatial resolution of the postseismic slip maximum was estimated as about 10 km along the fault. Pattern of patch A largely overlaps with an aseismic slip maximum around the hypocenter of the 1999 Izmit earthquake which was also observed by Burgmann et al. (2002) (Fig.10). This seems to be in contradiction with the common assumption that afterslip is limited to velocity strengthening zones. Interestingly, it was at this part of the Izmit rupture where an unexpected normal-faulting component and significant back-rotation in the local stress field orientation during the inter Izmit-Düzce phase has been observed (Ickrath et al., 2014). Iio et al. (2002) installed a dense network to monitor the aftershock activity along the Karadere segment. The authors observed that hypocenters are concentrated within a narrow depth range near the

bottom of the seismogenic layer. This is in good agreement with this study and modelled slip distribution based on GPS data by Reilinger et al. (2000). Burgmann et al. (2002) concluded that the maximum post-seismic slip accumulated beneath the Karadere segment during the first three months after the Izmit mainshock. It is suggested that post-Izmit afterslip may have loaded fault segments adjacent to the rupture and potentially triggered the 1999 Düzce earthquake.
Similar to the inter Izmit-Düzce period, the post-Düzce patches C+D (seismically inactive uppermost crust) overlap with the postseismic slip maxima below the brittle-ductile transition, respectively (Fig. 10).

In Figure 10 we summarize the observations obtained for coseismic slip distribution for both M>7 mainshocks, their aftershock distributions and the respective postseismic deformation below the seismogenic part of the crust along the combined Izmit-Düzce section of the North Anatolian Fault Zone extending from the surface down to the base of the crust. Distinct fault patches within the seismogenic upper crust that are seismically inactive during the inter Izmit-Düzce (A, B) and post Düzce (C, D) periods correspond to the postseismically deforming patches within the lower crust. The distribution of postseismic slip maxima and aftershocks in space and time indicate that the entire fault zone was activated within the time frame of ~2 years following the mainshocks. The coseismic rupture produced a heterogeneous slip distribution along the segmented fault. Aftershock activity in the upper crust and postseismic creep focused in the lower crust contribute to balance the slip distribution across the fault down to the upper mantle.

Shallow aftershocks on the western Düzce fault: A total of 195 shallow aftershocks (down to 3 km depth) were observed as part of the post Izmit and Düzce seismicity. These events are well-constrained on their focal depth and decoupled from the vast majority of Izmit and Düzce aftershocks. A clear concentration of these shallow earthquakes along the western tip of the Düzce fault can be observed (Fig. 11). The shallow seismicity occurred immediately after the Izmit earthquake and close to the eastern termination of the Izmit rupture. Interestingly, the shallow aftershocks do not follow an Omori decay after the two mainshocks but shows a strong temporal clustering around March 2000, eight and five months after the Izmit and Düzce mainshock, respectively. Furthermore, also the magnitude distribution of these events with time does not give any evidence for a mainshock-aftershock sequence, but rather suggest swarm-type behavior. A similar phenomenon has also been observed beyond the western rupture termination of the Izmit earthquake below the easternmost Sea of Marmara (Bulut et al., 2011; Prevedel et al., 2015; Raub et al., 2016). Inverting the P-wave polarities of the shallow events for the local stress field allows to derive a clear strike-slip regime for the uppermost kilometers at the junction from the Karadere to the Düzce faults. The obtained orientation for the maximum and minimum principal stresses clearly tends to favor the activation of an east-west striking vertical fault in a right-lateral sense and is thus in good accordance with the regional stress field (Kiratzi, 2002; Hurd & Bohnhoff, 2012; Eken et al., 2013; Ickrath et al., 2014; 2015).

Pucci et al. (2006; 2007) analyzed the postseismic slip distribution along the Düzce fault. They observed different slip distributions along the eastern and western parts of the fault, respectively. The western part shows almost no postseismic deformation and a simple linear co-seismically activated fault trace that has probably reactivated an older complex fault system. In contrast, along the eastern part of the fault the co-seismically activated fault trace crosses this older and complex fault system. The segmentation of the Düzce fault is also well reflected by the coseismic slip distribution at depth. Delouis et al. (2002) compared the shallow fault complexities with the slip distribution at depth. The comparison with the surface data by Pucci et al. (2006) shows an abrupt decrease of the coseismic slip at depth exactly at the boundary between the western and eastern part of the Düzce fault (Fig. 11). The western part of the fault hosted a slip maximum of 4.5 m at the surface during the Düzce earthquake, but, in contrast is dominated by a low-slip area at depth not exceeding 2 m. In contrast, the eastern part shows a coseismic slip maximum of locally eventually up to 8 m (Pucci et al., 2006). Interestingly, the observed shallow seismicity in this region exactly follows the subdivision of the Düzce fault in that shallow events tend to occur on its western portion while no single shallow events were located on its eastern portion.

Another observation to consider is the present-day subsidence of the southwestern part of the Düzce Basin which is not entirely fault-related and not an active pull-apart basin as a whole. In contrast, the northwestern part of the Düzce Basin is shrinking because of the transpressional deformation due to the Karadere fault (Pucci et al., 2006). Sibson (1985) and Harris & Day (1993; 1999) studied the phenomenon of rupture arrests of earthquakes. When differences in fluid pressure do not act as a barrier, the lower observed normal stress along the western Düzce fault may favor the rupture propagation. However, this would lower the rupture velocity and would lead to a delay of the triggering process on the neighboring fault segment. This could have played a role for the delayed triggering of the shallow events at this part of the rupture. Eventually it might even be a possible explanation for the delayed propagation of the Izmit rupture onto the Düzce fault (87 days delay) (Pucci et al., 2006). We conclude that the Eften Lake step-over on the western part of the Düzce fault might represent a barrier for the shallow earthquakes limiting their occurrence to the western side of the Düzce fault and at the same time potentially also played a role in the delayed rupture propagation of the Izmit rupture onto the Düzce fault.

5. Conclusions

The unique sequence of two consecutive M>7 earthquakes occurring on adjacent fault segments allowed to observe a clear spatiotemporal distribution of crustal seismicity in conjunction with co- and postseismic slip distribution on the brittle upper and ductile lower part of the crust, respectively. While the mainshocks acted as triggering aftershocks by 'switching on and off' particular fault patches in the upper half of the seismogenic layer (uppermost 10 km) there is a clear along-fault relation of the more shallow seismically active and inactive patches with the postseismic slip distribution. In contrast, no spatial correlation between the coseismic and postseismic slip distribution is observed. Incorporating the lateral variations of the local seismotectonic setting along the combined Izmit-Düzce rupture area (strike slip segments and pull-apart basins) it can be concluded that such structural features may be responsible for along-rupture variations of co- and postseismic deformation in conjunction with strong variations in shallow (<10 km deep) aftershock activity. Analyzing the cumulative distribution of coseismic slip, aftershock distribution and postseismic deformation throughout the entire seismogenic and ductile crust allows concluding that lateral and vertical variations in co- and postseismic deformation are temporal effects only and smoothed out on the long-term.

6. Acknowledgements

The study was funded by the Helmholtz Association in the frame of the Young Investigators Group ‘From Microseismicity to Large Earthquakes’. We thank Fatih Bulut for involvement in an early stage of the work and are thankful to Oliver Germer for his support during data processing and phase picking. We thank Stefan Bentz and Sophia Bohnhoff Blanco for contributing to the design of Figs. 2, 3, 10, and Christina Raub for compiling the hypocenter catalogue here provided as electronic supplement. We gratefully acknowledge the German Task Force for Earthquakes (GTF) and especially J. Zschau and C. Milkereit for providing the Izmit and Düzce aftershock waveform data from the GTF and Sapanca-Bolu (SABONET) seismic networks. Most of the figures were created with the GMT software (Wessel & Smith 1998). We thank one anonymous reviewer and the editor Jean-Philippe Avouac for constructive comments that helped to improve the manuscript.

7. References

Abers, G.A., Gephart, J.W., 2001. Direct inversion or earthquake first motions for both the stress tensor and focal mechanisms and application to southern California. J. Geophys. Res. 106(26), 26,523-26,540.

Aktar, M., Özalaybey, S., Ergin, M., Karabulut, H., Bouin, M.-P., Tapirdamaz, C., Biçmen, F., Yörük, A., Bouchon, M., 2004. Spatial variation of aftershock activity across the rupture zone of the 17 August 1999 Izmit earthquake, Turkey. Tectonophysics 391(1), 325-334.

Aydin, A., Kalafat, D., 2002. Surface ruptures of the 17 August and 12 November 1999 Izmit and Düzce earthquakes in northwestern Anatolia, Turkey: their tectonic and kinematic significance and the associated damage. Bull. Seismol. Soc. Am. 92(1), 95-106.

Akyüz, H., Hartleb, R., Barka, A.A., Altunel, E., Sunal, G., Meyer, B., Armijo, R., 2002. Surface rupture and slip distribution of the 12 November 1999 Düzce earthquake (M7.1), North Anatolian Fault, Turkey. Bull. Seismol. Soc. Am. 92(1), 61-66.

Avouac, J.-P., 2015. From Geodetic Imaging of Seismic and Aseismic Fault Slip to Dynamic Modeling of the Seismic Cycle. Annu. Rev. Earth Planet. Sci. 43:233-71, doi: 10.1146/annurev-earth-060614-105302.

Barka, A.A., 1992. The North Anatolian fault zone, Annales Tectonicae, Spec. Iss. VI, 164-195.

Barka, A.A., Akyüz, H., Altunel, E., Sunal, G., Cakir, Z., Dikbas, A., Yerli, B., Armijo, R., Meyer, B., de Chabalier, J., Rockwell, T., Dolan, J., Hartleb, R., Dawson, T., Christofferson, S., Tucker, A., Fumal, T., Langridge, R., Stenner, H., Lettis, W., Bachhuber, J., Page, W., 2002. The Surface Rupture and Slip Distribution of the 17 August 1999 Izmit Earthquake (M7.4), North Anatolian Fault. Bull. Seismol. Soc. Am. 92(1), 43-60.

Baumbach, M., Bindi, D., Grosser, H., Milkereit, C., Parolai, S., Wang, R., Karakisa, S., Zünbül, S., Zschau, J., 2003. Calibration of an ML scale in northwestern Turkey from 1999 Izmit aftershocks. Bull. Seismol. Soc. Am. 93(5), 2289-2295.

Bindi, D., Parolai, S., Gorgun, E., Grosser, H., Milkereit, C., Bohnhoff, M., Durukal, E., 2007. ML scale in northwestern Turkey from 1999 Izmit Aftershocks: Updates. Bull. Seismol. Soc. Am., 97(1B), 331-338.

BenZion, Y., Sammis, C.G., 2003. Characterization of fault zones. PAGEOPH 160, 677–715.

Bohnhoff, M., Harjes, H.-P., Meier, T., 2005. Deformation and stress regimes in the Hellenic subduction zone from focal Mechanisms, J. Seismol. 9, 341-366.

Bohnhoff, M., Grosser, H., Dresen, G., 2006. Strain partitioning and stress rotation at the North Anatolian fault zone from aftershock focal mechanisms of the 1999 Izmit Mw= 7.4 earthquake, Geophys. J. Int. 166(1), 373-385.

Bohnhoff, M., Bulut, F., Gorgün, E., Milkereit, C., Dresen, G., 2008. Seismotectonic setting at the North Anatolian Fault Zone after the 1999 Mw= 7.4 Izmit earthquake based on high-resolution aftershock locations. Adv. Geosc. 14, 85-92.

Bohnhoff, M., Bulut, F., Dresen, G., Malin, P.E., Eken, T., Aktar, M., 2013. An earthquake gap south of Istanbul, Nat. Commun. 4:1999, doi: 10.1038/ncomms2999.

Bohnhoff, M., Martínez-Garzón, P., Bulut, F., Stierle, E., Ben-Zion, Y., 2016. Maximum earthquake magnitudes along different sections of the North Anatolian fault zone. Tectonophysics, doi: 10.1016/j.tecto.2016.02.028.

Bouchon, M., Karabulut, H., 2008. The aftershock signature of supershear earthquakes. Science 320(5881), 1323-1325.

Bouchon, M., Karabulut, H., Aktar, M., Özalaybey, S., Schmittbuhl, J., Bouin, M.-P., 2011. Extended Nucleation of the Mw7.6 Izmit Earthquake. Science 331, 877, doi:10.1126/science.1197341.

Bouin, M.-P., Bouchon, M., Karabulut, H., Aktar, M., 2004. Geophys. J. Int. 159, 207-211.

Bos, A.G., Usai, S., Spakman, W., 2004. A joint analysis of GPS motions and InSAR to infer the coseismic surface deformation of the Izmit, Turkey earthquake. Geophys. J. Int. 158, 849-863.

Bulut, F., Aktar, M., 2007. Accurate relocation of Izmit earthquake (Mw= 7.4, 1999) aftershocks in Çinarcik Basin using double difference method. Geophys. Res. Lett. 34(10), L10307.

Bulut, F., Bohnhoff, M., Aktar, M., Dresen, G., 2007. Characterization of aftershock fault plane orientations of the 1999 Izmit (Turkey) earthquake using high-resolution aftershock locations. Geophys. Res. Lett. 34(20), L20306.

Bulut, F., Ellsworth, W.L., Bohnhoff, M., Aktar, M., Dresen, G., 2011 Spatiotemporal Earthquake Clusters along the North Anatolian Fault Zone Offshore Istanbul. Bull. Seismol. Soc. Am. 101(4), 1759-1768, doi: 10.1785/01200215.

Bulut, F., Ben-Zion, Y., Bohnhoff, M., 2012. Evidence for a bimaterial interface along the Mudurnu segment oft he North Anatolian Fault Zone from polarization analysis of P waves. Earth Planet. Sci. Lett., 327-328, 17-22.

Bulut, F., Bohnhoff, M., Eken, T., Janssen, C., Kilic, T., Dresen, G., 2012. The East Anatolian Fault Zone: Seismotectonic setting and spatiotemporal characteristics of seismicity based on precise earthquake locations. J. Geophys. Res. 117, B07304, doi: 10.1029/2011JB008966.

Burgmann, R., Dresen, G., 2008. Rheology of the lower crust and upper mantle: Evidence from rock mechanics, geodesy, and field observations. Annual Review of Earth and Planetary Sciences 36(1), 531.

Burgmann, R., Ergintav, S., Segall, P., Hearn, E., McClusky, S., Reilinger, R., Woith, H., Zschau, J., 2002. Time-Dependent Distributed Afterslip on and Deep below the Izmit Earthquake Rupture. Bull. Seismol. So. Am. 92(1), 126-137.

Çakir, Z., Barka, A. A., De Chabalier, J. B., Armijo, R., Meyer, B., 2003a. Kinematics of the November 12, 1999 (Mw= 7.2) Düzce earthquake deduced from SAR interferometry. Turkish Journal of Earth Sciences 12(1), 105-118.

Çakir, Z., Chabalier, J.-B. d., Armijo, R., Meyer, B., Barka, A., Peltzer, G., 2003b. Coseismic and early post-seismic slip associated with the 1999 Izmit earthquake (Turkey), from SAR interferometry and tectonic field observations. Geophys. J. Int. 155(1), 93-110.

Chang, S.-H., Avouac, J.-P., Barbot, S., Lee, J.-C., 2013. Spatially variable fault friction derived from dynamic modeling of aseismic afterslip due to the 2004 Parkfield earthquake. J. Geophys. Res. 118, 3431-3447.

Delouis, B., Giardini, D., Lundgren, P., Salichon, J., 2002. Joint inversion of InSAR, GPS, teleseismic, and strong-motion data for the spatial and temporal distribution of earthquake slip: Application to the 1999 Izmit mainshock. Bull. Seismol. Soc. Am. 92(1), 278-299.

Eken, T., Bohnhoff, M., Bulut, F., Can, B., Aktar, M., 2013. Crustal Anisotropy in the Eastern Sea of Marmara Region in Northwestern Turkey, Bull. Seism. Soc. Am. 103, 911-924.

Ergintav, S., McClusky, S., Hearn, E., Reilinger, R., Cakmak, R., Herring, T., Ozener, H., Lenk, O., Tari, E., 2009. Seven years of postseismic deformation following the 1999, M= 7.4 and M= 7.2, Izmit-Düzce, Turkey earthquake sequence. J. Geophys. Res. 114(B7), B07403, doi:10.1029/2008JB006021.

Feigl, K.L., Sarti, F., Vadon, H., McClusky, S., Ergintav, S., Durand, P., Burgmann, R., Rigo, A., Massonnet, D., Reilinger, R., 2002. Estimating Slip Distribution for the İzmit Mainshock from Coseismic GPS, ERS-1, RADARSAT, and SPOT Measurements. Bull. Seismol. Soc. Am. 92(1), 138-160.

Flerit, F., Armijo, R., King, G., Meyer, B., 2004. The mechanical interaction between the propagating North Anatolian Fault and the back-arc extension in the Aegean, Earth Planet. Sci. Lett. 224, 347-362.

Goebel, T. H. W., Becker, T. W., Sammis, C. G., Dresen, G., Schorlemmer, D., 2014a. Off-fault damage and acoustic emission distributions during the evolution of structurally complex faults over series of stick-slip events. Geophys. J. Int. 197(3), 1705-1718.

Goebel, T. H. W., Candela, T., Sammis, C. G., Becker, T. W., Dresen, G., Schorlemmer, D., 2014b. Seismic event distributions and off-fault damage during frictional sliding of saw-cut surfaces with pre-defined roughness. Geophys. J. Int. 196(1), 612-625.

Görgün, E., Zang, A., Bohnhoff, M., Milkereit, C., Dresen, G., 2009. Analysis of Izmit aftershocks 25 days before the November 12th 1999 Düzce earthquake, Turkey. Tectonophysics 474(3-4), 507-515.

Görgün, E., Bohnhoff, M., Bulut, F., Dresen, G., 2010. Seismotectonic setting of the Karadere-Düzce branch of the North Anatolian Fault Zone between the 1999 Izmit and Düzce ruptures from analysis of Izmit aftershock focal mechanisms. Tectonophysics 482, 170-181.

Gülen, L., Pinar, A., Kalafat, D., Özel, N., Horasan, G., Yilmazer, M., Işıkara, A. M., 2002. Surface fault breaks, aftershock distribution, and rupture process of the 17 August 1999 Izmit, Turkey, earthquake. Bull. Seismol. Soc. Am. 92(1), 230-244.

Harris, R. A., Day, S. M., 1993. Dynamics of fault interaction: Parallel strike-slip faults. J. Geophys. Res. 98(B3), 4461-4472.

Harris, R. A., Day, S. M., 1999. Dynamic 3d simulations of earthquakes on en echelon faults. Geophys. Res. Lett. 26(14), 2089-2092.

Hearn, E. H., Bürgmann, R., Reilinger, R. E., 2002. Dynamics of Izmit earthquake postseismic deformation and loading of the Düzce earthquake hypocenter. Bull. Seismol. Soc. Am. 92(1), 172-193.

Hearn, E., McClusky, S., Ergintav, S., Reilinger, R., 2009. Izmit earthquake postseismic deformation and dynamics of the North Anatolian Fault Zone. J. Geophys. Res. 114(B8), B08405, doi:10.1029/2008JB006026.

Hurd, O., Bohnhoff, M., 2012. Stress- and Structure-Induced Shear-Wave Anisotropy along the 1999 Izmit Rupture, Northwest Turkey. Bull. Seismol. Soc. Am., 102(5), 2177-2188, doi: 10.1785/0120110270.

Ickrath, M., 2015. Spatiotemporal variations of the local stress field and fault asperities at the North Anatolian Fault in NW Turkey analysed based on microseismic recordings, Dissertation. http://www.diss.fu-berlin.de/diss/receive/FUDISS_thesis_000000098214.

Ickrath, M., Bohnhoff, M., Bulut, F., Dresen, G., 2014. Stress rotation and recovery in conjunction with the 1999 Izmit Mw 7.4 earthquake. Geophys. J. Int. 196(2), 951-956.

Ickrath, M., Bohnhoff, M., Dresen, G., Bulut, F., Martínez-Garzón, P., Kwiatek, G., Germer, O., 2015. Detailed Analysis of Spatiotemporal Variations of the Stress Field Orientation Along the

Izmit-Düzce Rupture in Nw Turkey from Inversion of First-Motion Polarity Data. Geophys. J. Int. 202(3), 2120-2132.

Iio, Y., Horiuchi, S., Bariş, Ş., Celik, C., Kyomen, J., Üçer, B., Honkura, Y., Işikara, A.M., 2002. Aftershock distribution in the eastern part of the aftershock region of the 1999 Izmit, Turkey, earthquake. Bull. Seismol. Soc. Am. 92(1), 411-417.

Kiratzi, A. A., 2002. Stress tensor inversions along the westernmost North Anatolian fault zone and its continuation into the North Aegean sea. Geophys. J. Int. 151(2), 360-376.

Konca, A.O., Leprince, S., Avouac, J.-P., Helmberger, D.V., 2010. Rupture Process of the 1999 Mw 7.1 Duzce Earthquake from Joint Analysis of SPOT, GPS, InSAR, Strong-Motion, and Teleseismic Data: A Supershear Rupture with Variable Rupture Velocity. Bull. Seismol. Soc. Am. 100(1), 267-288.

Lee, W., Lahr, J., 1972. HYPO-71 a computer program for determining hypocenter, magnitude and first motion pattern of local earthquakes, Open-File Report. US Geol. Surv., Menlo Park, Calif.

Le Pichon, X.L., Şengör, A.M.C., Kende, J., İmren, C., Henry, P., Grall, C., Karabulut, H., 2015. Propagation of a strike slip plate boundary within an extensional environment: the westward propagation of the North Anatolian Fault, *Can. J. Earth Sci.* doi 10.1139/cjes-2015-0129. [online] Available from: http://www.nrcresearchpress.com/doi/abs/10.1139/cjes-2015-0129 (Accessed 4 January 2016)

Lienert, B. R. Havskov, J., 1995. A computer program for locating earthquakes both locally and globally, Seismol. Res. Lett. 66(5), 26-36.

Lienert, B. R., Berg, E., Frazer, L.N., 1986. HYPOCENTER: An earthquake location method using centered, scaled, and adaptively damped least squares. Bull. Seismol. Soc. Am. 76(3), 771-783.

McClusky, S., S. Balassanian, A. Barka, C. Demir, S. Ergintav, I. Georgiev, O. Gurkan, M. Hamburger, K. Hurst, H. Kahle, K. Kastens, G. Kekelidze, R. King, V. Kotzev, O. Lenk, S. Mahmoud, A. Mishin, M. Nadariya, A. Ouzounis, D. Paradissis, Y. Peter, M. Prilepin, R. Reilinger, I. Sanli, H. Seeger, A. Tealeb, M. N. Toksöz and G. Veis, 2000. Global Positioning System constraints on plate kinematics and dynamics in the eastern Mediterranean and Caucasus. J. Geophys. Res. 105, 5695-5719.

Meghraoui, M., Aksoy, M. E., Akyüz, H. S., Ferry, M., Dikba, A., Altunel, E.,

2012. Paleoseismology of the North Anatolian Fault at Güzelköy (Ganos segment, Turkey): Size and recurrence time of earthquake ruptures west of the Sea of Marmara. Gcubed 13(4).

Milkereit, C., Zünbül, S., Karakisa, S., Iravul, Y., Zschau, J., Baumbach, M., Grosser, H., Günther, E., Umutlu, N., Kuru, T., 2000. Preliminary aftershock analysis of the Mw= 7.4 Izmit and Mw= 7.1 Düzce earthquake in western Turkey. In Barka, A., editor, The 1999 Izmit and Düzce Earthquakes: Preliminary Results, pages 179-187, Istanbul Tech. Univ., Istanbul, Turkey.

Najdahmadi, B., Bohnhoff, M., Ben-Zion, Y., Bimaterial interfaces at the Karadere segment of the North Anatolian Fault, northwestern Turkey. J. Geophys. Res., in press, 2016.

Özalaybey, S., Ergin, M., Aktar, M., Tapirdamaz, C., Bicman, F., Yörük, A., 2002. The 1999 Izmit earthquake sequence in Turkey: Seismological and Tectonic Aspects. Bull. Seismol. Soc. Am. 92(1), 376-386.

Perfettini, H., Acouac, J.-P., 2004. Stress transfer and strain rate variations during the seismic cycle. J. Geophys. Res., 109, B06402, doi:10.1029/2003JB002917.

Perfettini, H., Avouac, J.-P., 2007. Modeling afterslip and aftershocks following the 1992 Landers earthquake. J. Geophy. Res. 112, B07409, doi:10.1029/2006JB004399.

Prevedel, B., Bulut, F., Bohnhoff, M., Raub, C., Kartal, R.F., Alver, F., Malin, P.E., 2015. Downhole Geophysical Observatories: Best Installation Practices and a Case History from Turkey. Int. J.Earth Sci , doi: 10.1007/s00531-015-1147-5.

Polat, O., Eyidogan, H., Haessler, H., Cisternas, A., Philip, H., 2002. Analysis and interpretation of the aftershock sequence of the August 17, 1999, Izmit (Turkey) earthquake, J. Seismol. 6, 287–306.

Pucci, S., Pantosti, D., Barchi, M., Palyvos, N., 2006. Evolution and complexity of the seismogenic Düzce fault zone (Turkey) depicted by coseismic ruptures, Plio-Quaternary structural pattern and geomorphology. Geophys. Res. Abstr. 8, 08339.

Pucci, S., Pantosti, D., Barchi, M. R., Palyvos, N., 2007. A complex seismogenic shear zone: The Düzce segment of North Anatolian Fault (Turkey). Earth Planet. Sci. Lett. 262(1-2), 185-203.

Raub, C., Bohnhoff, M., Petrovic, B., Parolai, S., Malin, P.E., Yanik, K., Kartal, R.F., Kiliç, T. Seismic wave propagation in shallow layers at the GONAF-Tuzla site, Istanbul, Turkey, Bull. Seismol. Soc. Am. 106(3), 912–927, doi:10.1785/0120150216.

Reid, H., 1910. Permanent displacements of the ground, The California Earthquake of April, 18, 1906. Report of the State Earthquake Investigation Commission,Washington. Seismic travel and near surface crustal velocity structure bounding the San Andreas Fault zone near Parkfield, California.

Reilinger, R. E., Ergintav, S., Burgmann, R., McClusky, S., Lenk, O., Barka, A., Gurkan, O., , 2000. Coseismic and postseismic fault slip for the 17 August 1999, M= 7.5, Izmit, Turkey earthquake. Science 289(5484), 1519.

Reilinger, R., McClusky, S., Vernant, P., Lawrence, S., Ergintav, S., Cakmak, R., Ozener, H., Kadirov, F., Guliev, I., Stepanyan, R., Nadariya, M., Hahubia, G., Mahmoud, S., Sakr, K., ArRajehi, A., Paradissis, D., Al-Aydrus, A., Prilepin, M., Guseva, T., Evren, E., Dmitrotsa, A., Filikov, S.V., Gomez, F., Al-Ghazzi, R., Karam, G., 2006. GPS constraints on continental deformation in the Africa-Arabia-Eurasia continental collision zone and implications for the dynamics of plate interactions. J. Geophys. Res. 111, B05411, doi:10.1029/2005JB004051.

Rolandone, F., Bürgmann, R., Nadeau, R., 2004. The evolution of the seismic-aseismic transition during the earthquake cycle: Constraints from the time-dependent depth distribution of aftershocks. Geophys. Res. Lett. 31(23).

Rolandone, F., Jaupart, C., Mareschal, J., Gariépy, C., Bienfait, G., Carbonne, C., Lapointe, R., 2002. Surface heat flow, crustal temperatures and mantle heat flow in the Proterozoic Trans-Hudson Orogen, Canadian Shield. J. Geophys. Res. 107(B12):ETG-7.

Saroglu, F., 1985. Dogu Anadolu nun Neotektonik Dönemde Jeolojik ve Yapsal Evrimi. PhD thesis. Istanbul Univ., Fen Bilim. Enst., Istanbul. 240 pp.+ 7 foldouts.

Saroglu, F., Emre, Ö., and Kuscu, 1992. Active fault map of turkey. General Directorate of Mineral Research and Exploration, Ankara.

Schildgen, T., Cosentino, D., Caruso, A., Buchwaldt, R., Yildirim, C., Bowring, S. A., Rojay, B., Echtler, H., Strecker, M., 2012. Surface expression of eastern Mediterranean slab dynamics: Neogene topographic and structural evolution of the southwest margin of the central Anatolian plateau, Turkey. Tectonics 31(2).

Scholz, C. H., 2002. TheMechanics of Earthquakes and Faulting, 2nd ed., Cambridge Univ. Press, Cambridge, U. K., doi:10.1017/S0016756803227564.

Segall, P., Burgmann, R., Matthews, M., 2000. Time-dependent triggered afterslip following the 1989 Loma Prieta earthquake. J. Geophys. Res. 105(B3), 5615-5634.

Sengör, A., Tüysüz, O., Imren, C., Sakinç, M., Eyidogan, H., Görür, N., Le Pichon, X., Rangin, C., 2005. The north Anatolian fault: A new look. Annu. Rev. Earth Planet. Sci. 33, 37-112. .

Sibson, R. H., 1985. Stopping of earthquake ruptures at dilational fault jogs. Nature 316(6025), 248-251.

Stierle, E, Vavryčuk. V., Šílený, J., Bohnhoff, M. 2014a. Resolution of Non-Double-Couple Components in the Seismic Moment Tensor Using Regional Networks—I: A Synthetic Case Study. Geophys. J. Int. 196(3), 1878-1888.

Stierle, E., Bohnhoff, M., Vavryčuk, V.,2014. Resolution of non-double-couple components in the seismic moment tensor using regional networks - II : application to aftershocks of the 1999 Mw 7.4 Izmit earthquake.Geophys. J. Int. 196(3), ggt502.

Thatcher, W., 1983. Nonlinear strain buildup and the earthquake cycle on the San Andreas fault. J. Geophys. Res. 88(B7), 5893-5902.

Tibi, R., Bock, G., Xia, Y., Baumbach, M., Grosser, H., Milkereit, C., Karakisa, S., Zünbül, S., Kind, R., Zschau, J., 2001. Rupture processes of the 1999 August 17 Izmit and November 12 Düzce (Turkey) earthquakes. Geophys. J. Int. 144(2), F1-F7.

Tse, S.T., Rice, J.R., 1986. Crustal earthquake instability in relation to the depth variation of frictional slip properties. J. Geophys. Res. 91(B9), 9452-9472.

Umutlu, N., Koketsu, K., Milkereit, C., 2004. The rupture process during the 1999 Düzce, Turkey, earthquake from joint inversion of teleseismic and strong-motion data. Tectonophysics 391(1-4), 315-324.

Waldhauser, F., Ellsworth, W. L., 2000. A double-difference earthquake location algorithm: method and application to the northern Hayward fault, California. Bull. Seismol. Soc. Am. 90(6), 1353.

Wessel, P., Smith, W. H. F., 1998. New, improved version of generic mapping tools released. Eos Trans. AGU 79(47), 579–579, doi:10.1029/98EO00426.

8. Figure Captions

Figure 1:

a) Topographic map of the North Anatolian Fault Zone (NAFZ) in northwestern Turkey with the main tectonic and geological units including the surface rupture of the two M>7 Izmit and Düzce earthquakes of 1999. Faults are taken from Meghraoui et al. (2012). Fault plane solutions for the Izmit and Düzce events from Tibi et al. (2001) and surface ruptures after Barka et al. (2002). Inset: Regional tectonic setting of the Mediterranean Sea and GPS-derived relative plate motions with respect to stable Eurasia (black arrows) for the Anatolian and Arabian plates. EAF- East Anatolian Fault, DSF - Dead Sea Fault. Black lines indicate major tectonic plate boundaries. Faults modified after Schildgen et al. (2012).

b) Station map of the SApanca-BOlu NETwork (SABONET) along the Izmit and Düzce ruptures. Surface ruptures are indicated by the dotted light and dark red lines. Faults as in a) and after Saroglu (1985). Yellow triangles are individual seismic stations with the station names. Stations HEN and CND are discussed later in the text and in Fig. 9.

Figure 2:

a) Mapped and modeled right-lateral coseismic surface slip of the 08/17/1999 Mw7.4 Izmit earthquake and an average model derived from the different studies. From top to bottom the graphs are after Barka et al. (2002) (field observations), Reilinger et al. (2000) (GPS data), Polat et al. (2002) (field observations), Bos et al. (2004) (modeled after GPS and InSAR data), Tibi et al. (2001) (GPS data), and the average slip which is used in the following for comparison with aftershock seismicity.

b) Averaged model of right-lateral coseismic slip distribution on the rupture plane during the Izmit earthquake. The shown slip distribution was derived from averaging published data from InSAR, GPS, teleseismic, and strong-motion data (Delouis et al., 2002) and GPS, ERS-1, RADARSAT, and SPOT measurements (Feigl et al., 2002).

c) Averaged model of right-lateral post-seismic creep at depth for the first 60 – 75 days following the Izmit earthquake. The postseismic creep distribution was derived from averaging published data from GPS data (Reilinger et al., 2000; Ergintav et al., 2009), and from a three-dimensional viscoelastic finite element method fit to later GPS data (Hearn et al., 2009).

Figure 3:

a) Mapped and modeled right-lateral coseimic surface slip of the 11/12/1999 Düzce Mw7.1 earthquake and an average model derived from the different studies. From top to bottom the graphs are after Akyüz et al. (2002) (field observations), Konca et al. (2010) (correlating SPOT images), Tibi et al. (2001) (GPS data), and the average slip which is used in the following for comparison with aftershock seismicity.

b) Averaged model of right-lateral coseismic slip distribution on the rupture plane during the Düzce earthquake. The shown slip distribution was derived from averaging published data from GPS and InSAR data (Burgmann et al., 2002), teleseismic and strong-motion data (Umutlu et al., 2004), and strong-motion and GPS data (Bouin et al., 2004).

c) Averaged model of right-lateral post-seismic creep at depth for the 1-2 years following the Düzce (and thus also the Izmit) earthquake. The postseismic creep distribution was derived from averaging published data from GPS data (Ergintav et al., 2009), and from a three-dimensional viscoelastic finite element method fit to later GPS data (Hearn et al., 2009).

Figure 4:

Temporal evolution of local seismicity along the combined Izmit/Düzce rupture. The hypocenter catalogue analyzed in this paper consists of different subdata sets that are color-coded in black (SABONET, absolute hypocenters, Ickrath et al., 2015), blue (SABONET, relocated hypocenters, newly compiled in this study) and green (densified network, relocated hypocenters, Bulut et al. (2007)), respectively. Earthquakes are plotted with geographical longitude since the surface ruptures of the Izmit and Düzce mainshocks extends east-west in first order approximation.

Figure 5:

Seismicity distribution along the Izmit/Düzce rupture in map view (upper part) and depth section (lower part) for the time period 1997-1999, prior to the Izmit Aug17, 1999 mainshock. We refer to this phase as ‘preseismic’ throughout the text. The red stars show the epicenters of the Izmit (left) and Düzce (right) earthquakes, respectively. The dashed lines indicate the surface ruptures of both events.

Figure 6:

Seismicity and slip distribution along the Izmit rupture for the ‘inter Izmit-Düzce’ phase (Aug17-Nov11, 1999). a) Mapped surface rupture of the Izmit mainshock modified after Aydin and Kalafat (2002). b) Spatial distribution of local seismicity along the Izmit rupture in map view (upper part) and depth section (lower part). Red dots indicate well-located shallow earthquakes as discussed in the text and shown in Fig. 11. Areas A and B indicate seismically inactive fault patches during the ‘inter Izmit-Düzce’ phase discussed in the text. The red stars show the locations of the Izmit (left) and Düzce (right) earthquakes, respectively.

Figure 7:

Seismicity and slip distribution along the Izmit/Düzce rupture for the ‘postseismic’ phase. a) Mapped surface rupture of the Düzce mainshock modified after Aydin and Kalafat (2002). b) Spatial distribution of local seismicity along the Izmit/Düzce rupture for the Düzce postseismic phase in map view (upper part) and depth section (lower part). Red dots indicate well-located shallow earthquakes as discussed in the text and shown in Fig. 11. Areas C and D indicate seismically inactive fault patches after the Düzce event discussed in the text. The red stars show the locations of the Izmit (left) and Düzce (right) earthquakes, respectively.

Figure 8:

Enlarged depth section of the four seismically inactive fault patches A-D and surrounding seismicity as shown in figures 4 and 5 for the inter Izmit-Düzce (upper part) and postseismic (lower part) phase. Grey bars represent the vertical and horizontal errors of the hypocenters, respectively, clearly indicating that the absence of seismicity within the patches A-D is significant.

Figure 9:

S-P differential times versus hypocentral distance for the two SABONET stations CND and HEN located closest to the 195 shallow earthquakes (see Fig. 1b for station locations and red crosses in Figure 8 for hypocenter locations). The S-P times document that these events are very shallow since the average velocity deduced from the slopes within the plots (red line) fits well the local velocity in the uppermost few kilometers. Figure after Ickrath (2014).

Figure 10:

Combined distribution of the Izmit (a) and Düzce (b) coseismic slip (upper Figures), aftershock density (middle Figures), and postseismic deformation (lower Figures). along the combined Izmit-Düzce section of the North Anatolian Fault Zone. Red dots indicate the Izmit and Düzce hypocenters, repspectively. Grey-shaded areas reflect the co- and postseismic deformation as in Figs. 2+3. Fault patches A-D within the seismogenic upper crust that are seismically inactive areas during the inter Izmit-Düzce (A, B) and post-Düzce (C. D) aftershock periods are indicated in each subfigure for orientation. The complementary distribution of seismically and aseismically deforming areas in space and time indicates that the entire (brittle and ductile) crust is being activated within the time frame of ~2 years following the two mainshocks.

Figure 11:

Distribution of shallow earthquakes along the Karadere and western Düzce segment in map view (upper part) and as depth section (lower part). The color coding indicates events during the years 1999 (blue) and 2000 (red), respectively. Fault lines are taken from Saroglu et al. (1992). The coseismic surface slip of the Düzce event is shown in the inset modified after Pucci et al. (2006). The arrows indicate the right-lateral strike-slip motion of the Düzce fault. The subfigure in the upper left shows the stress inversion result based on the MOTSI method (Abers & Gephard, 2001; see Ickrath et al., 2015 for details) indicating a strike-slip regime for the uppermost few kilometers. Figure after Ickrath (2014).

9. Figures

Figure 1a)

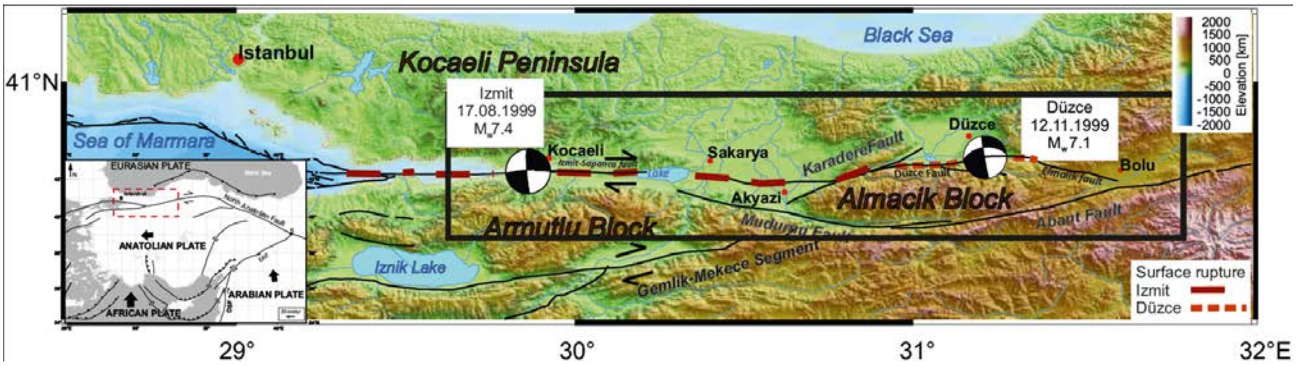

Figure 1b)

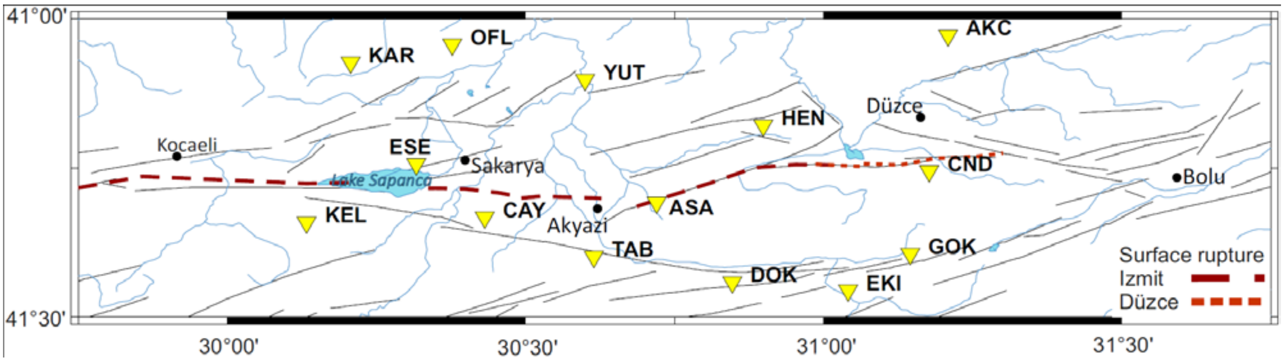

Figure 2a):

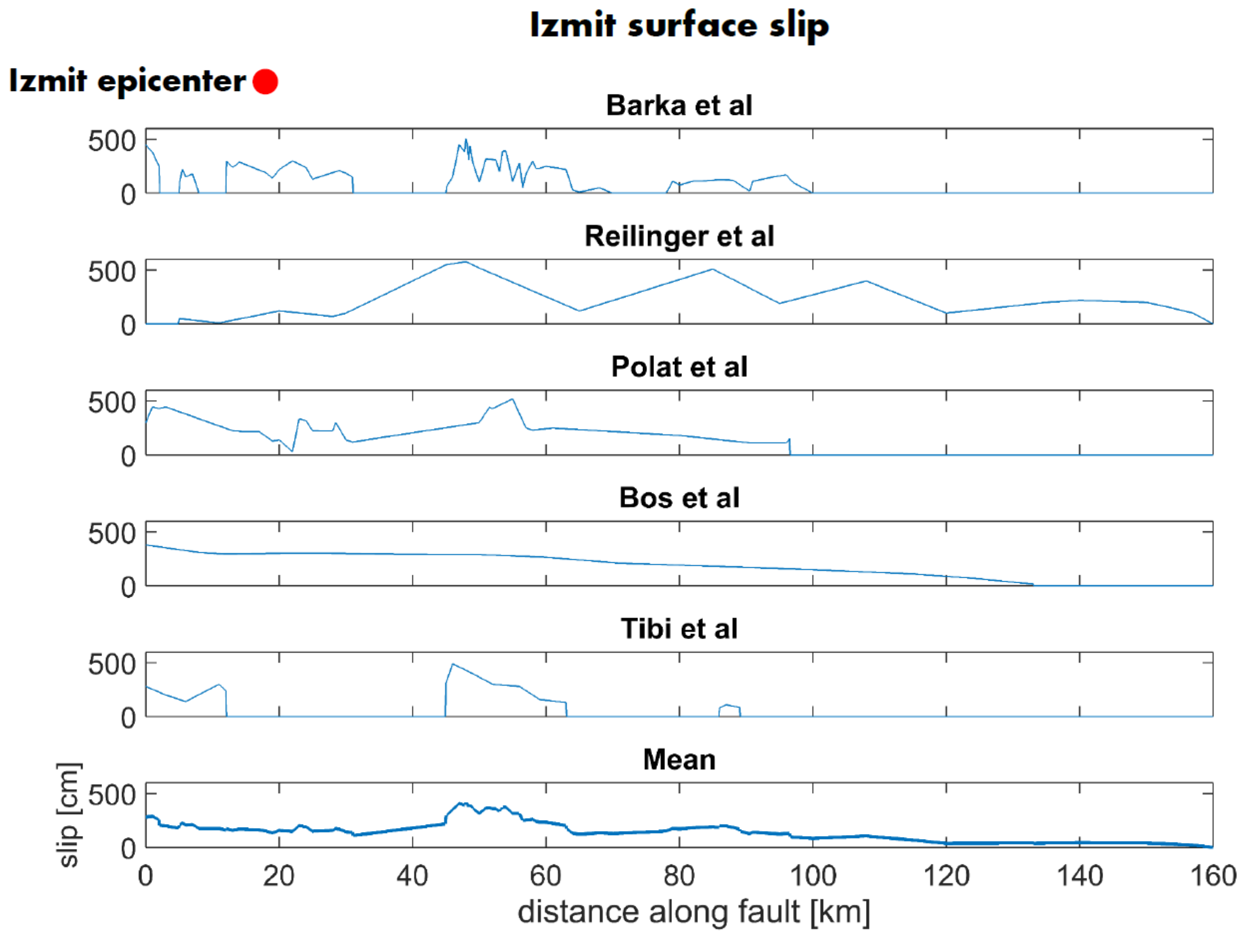
Izmit surface slip
Izmit epicenter
Barka et al
Reilinger et al
Polat et al
Bos et al
Tibi et al
Mean
500
0
slip [cm]
0
20
40
60
80
100
120
140
160
distance along fault [km]

Figure 2b):

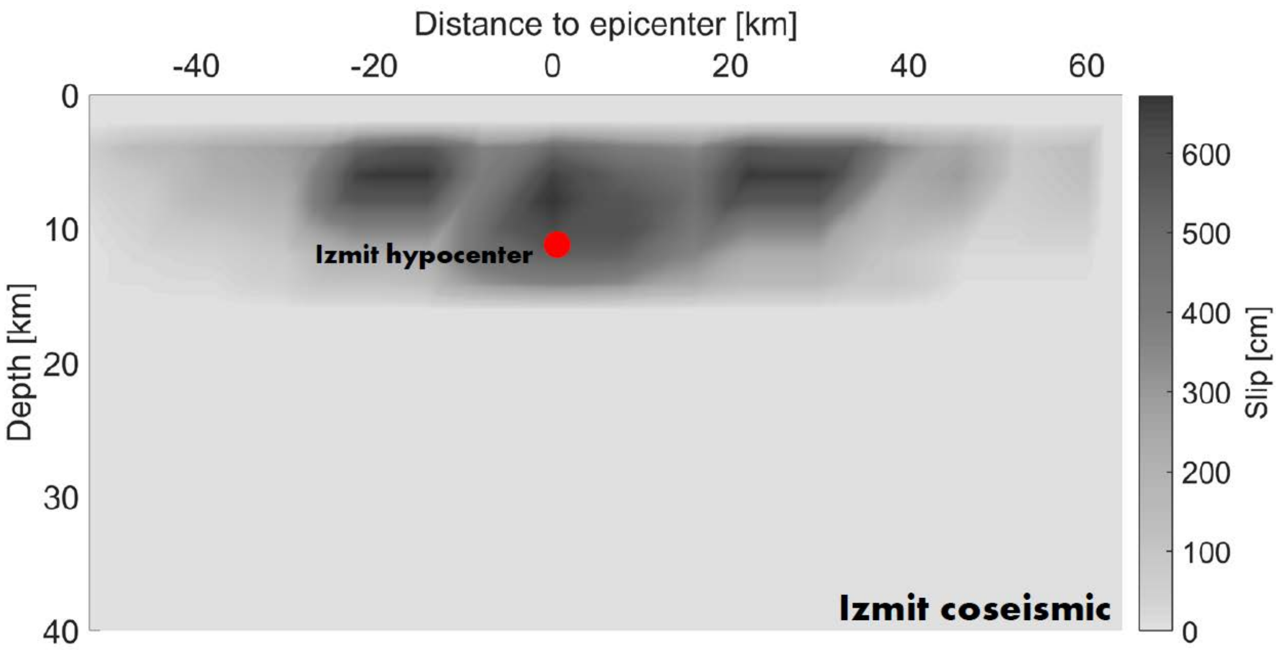

Figure 2c):

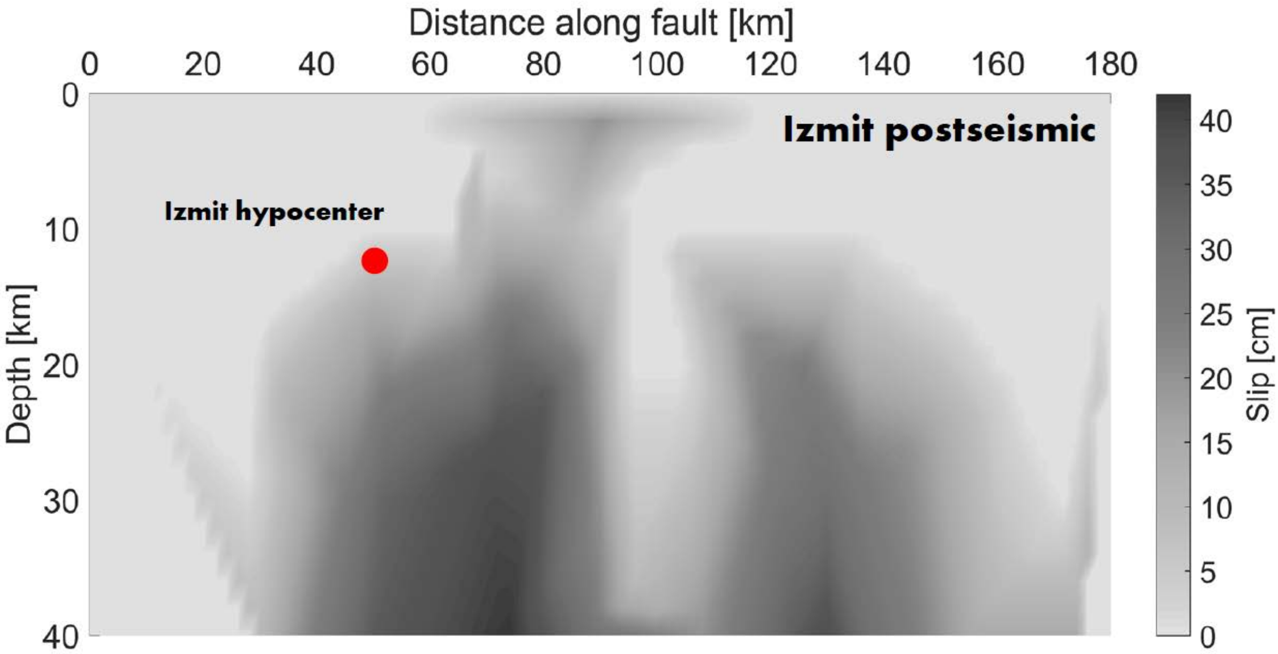

Figure 3a):

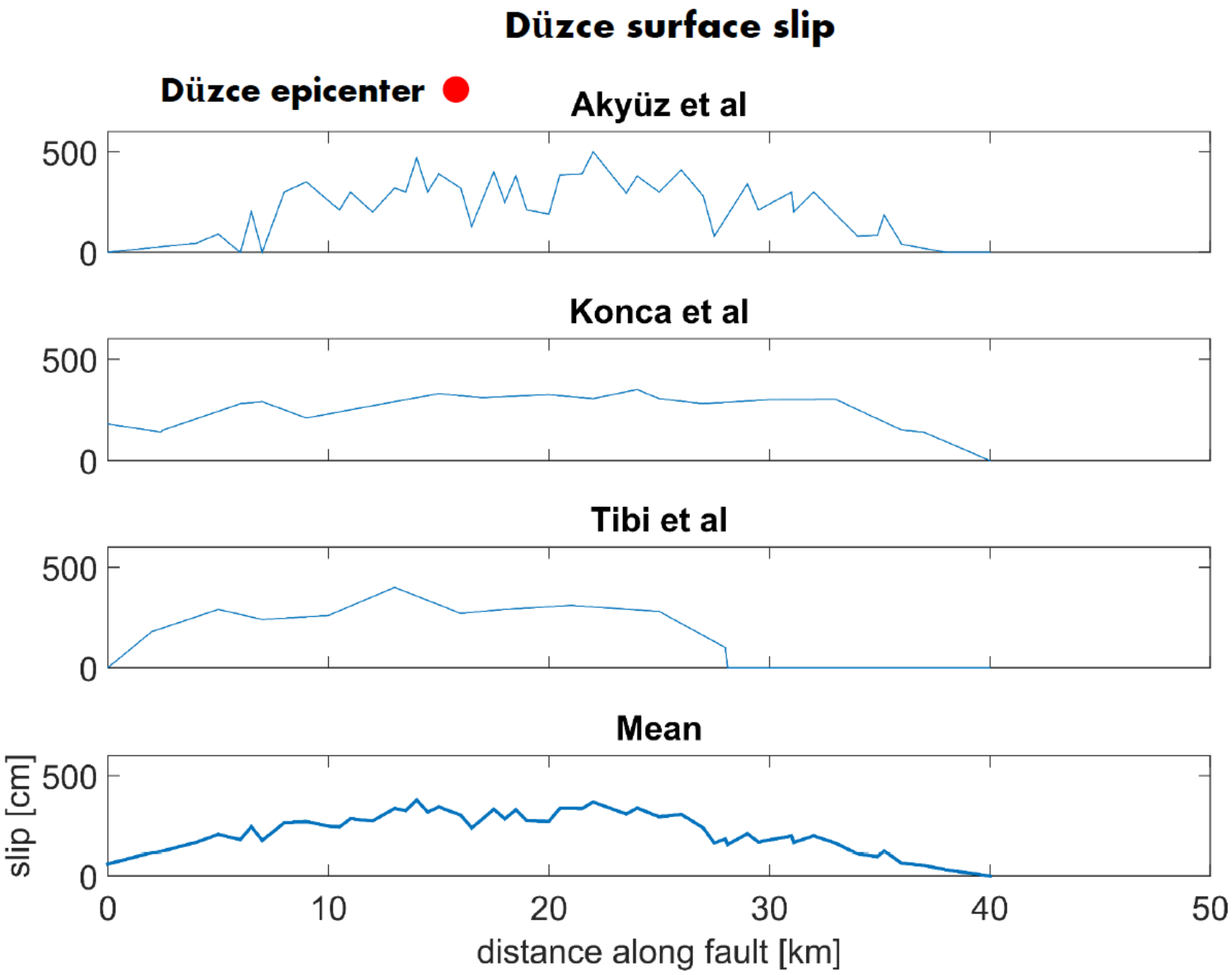
Düzce surface slip
Düzce epicenter
Akyüz et al
Konca et al
Tibi et al
Mean
slip [cm]
500
0
0
10
20
30
40
50
distance along fault [km]

Figure 3b):

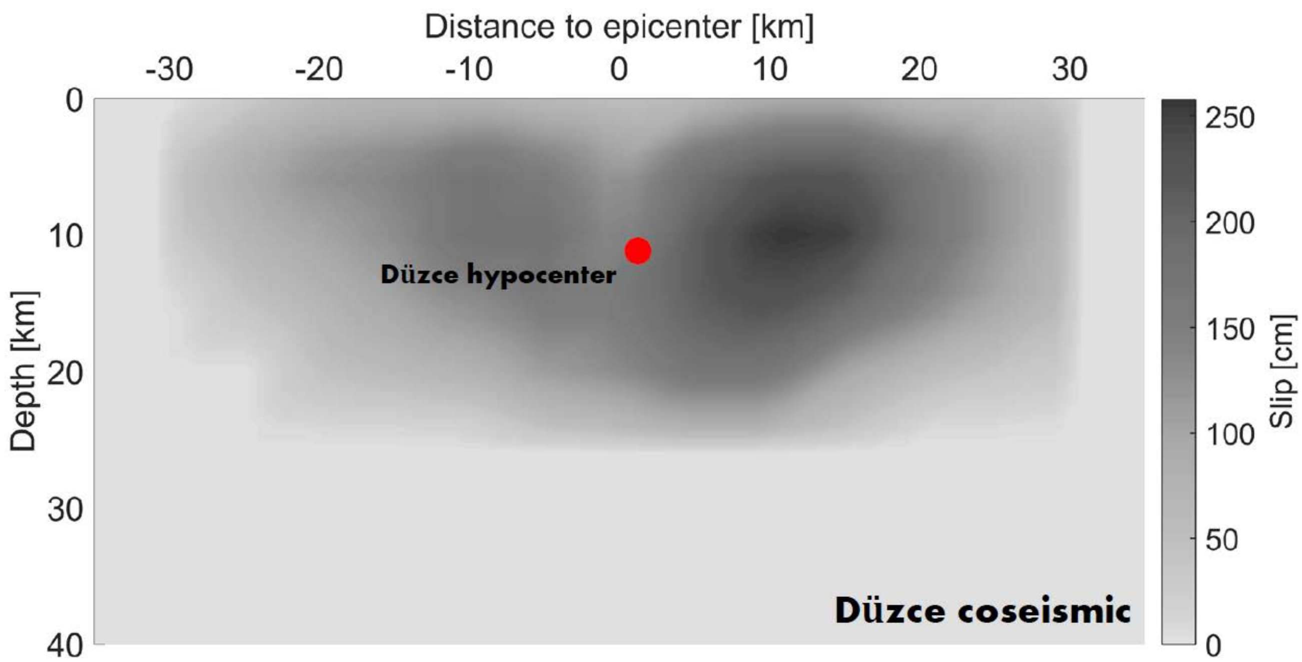

Figure 3c):

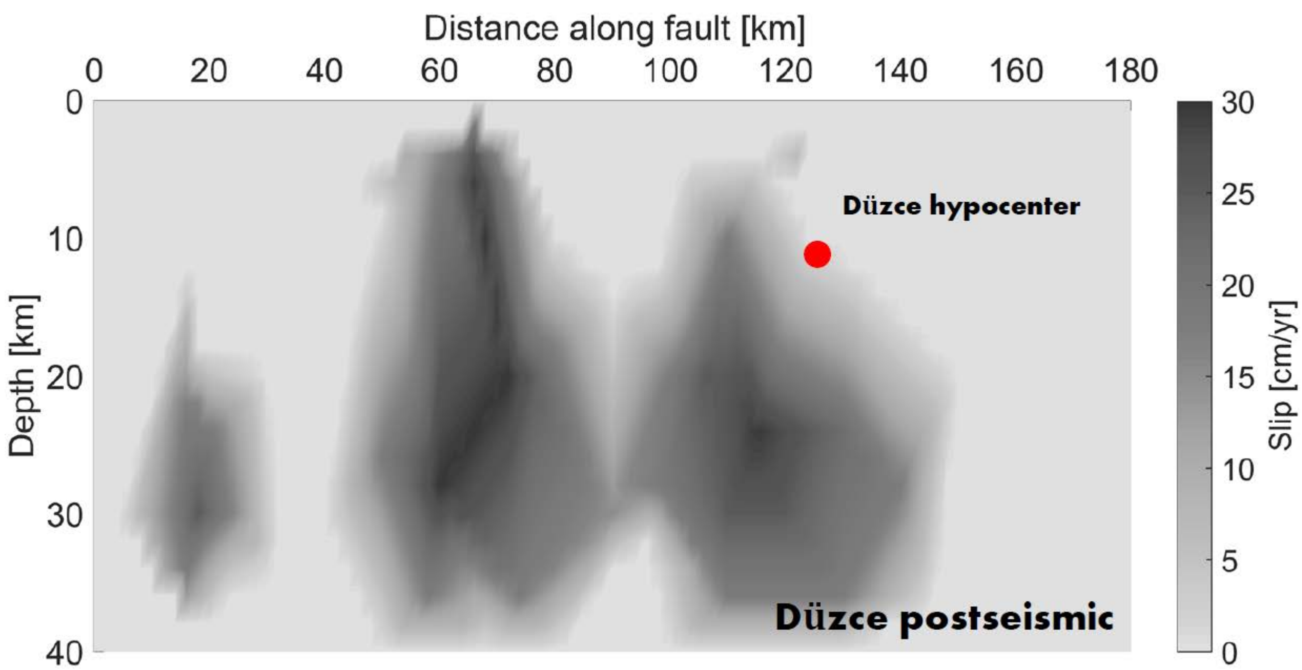

Figure 4

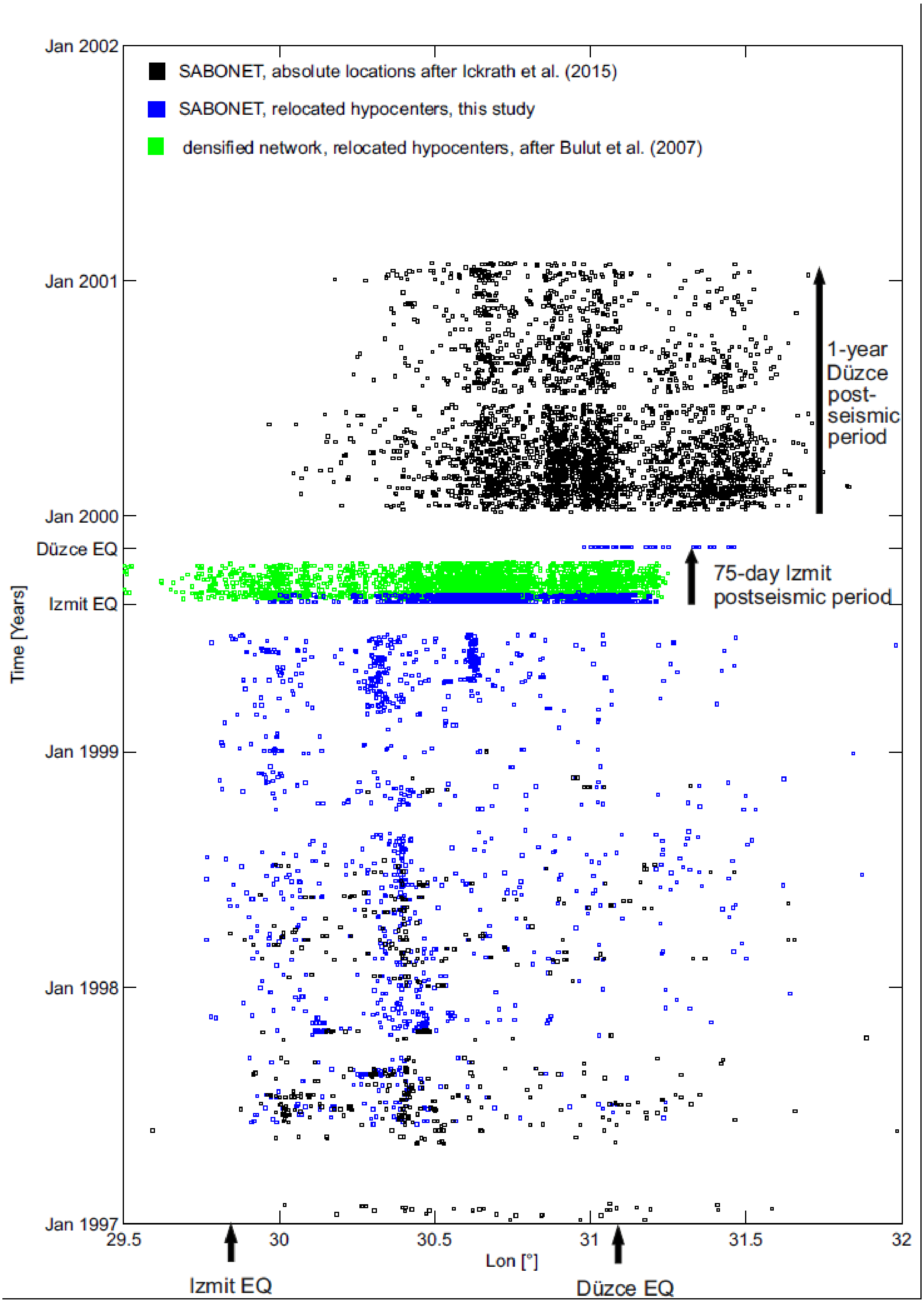

SABONET, absolute locations after Ickrath et al. (2015)
SABONET, relocated hypocenters, this study
densified network, relocated hypocenters, after Bulut et al. (2007)
Jan 2002
Jan 2001
Jan 2000
Düzce EQ
Izmit EQ
Jan 1999
Jan 1998
Jan 1997
Time [Years]
1-year Düzce post-seismic period
75-day Izmit postseismic period
29.5
30
30.5
31
31.5
32
Lon [°]
Izmit EQ
Düzce EQ

Figure 5

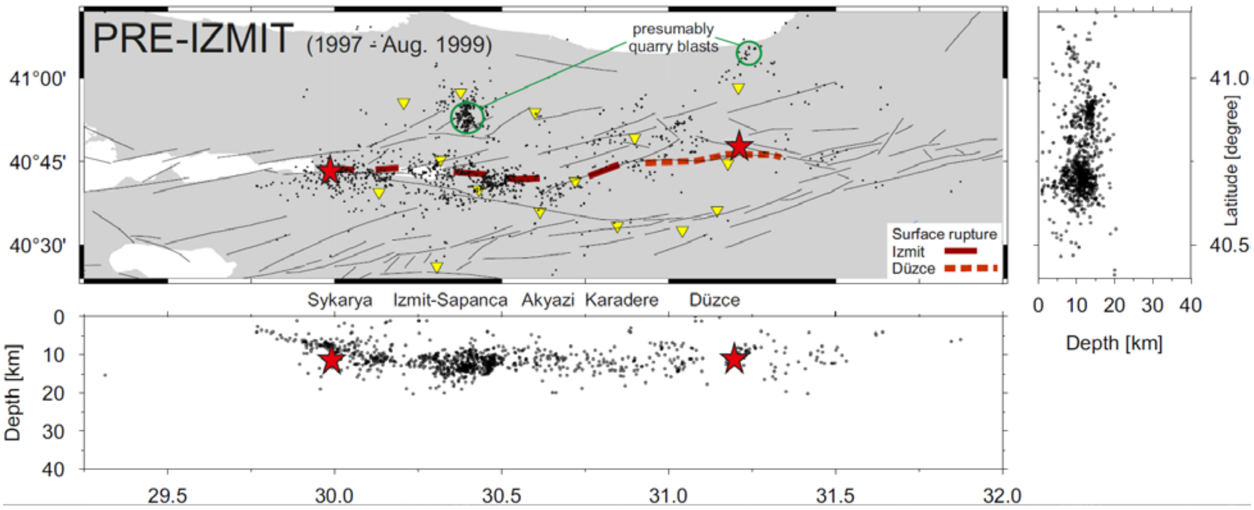
PRE-IZMIT (1997 - Aug. 1999)
presumably quarry blasts
41°00'
40°45'
40°30'
Surface rupture
Izmit
Düzce
Sykarya
Izmit-Sapanca
Akyazi
Karadere
Düzce
Depth [km]
0
10
20
30
40
29.5
30.0
30.5
31.0
31.5
32.0
41.0
40.5
Latitude [degree]
Depth [km]

Figure 6

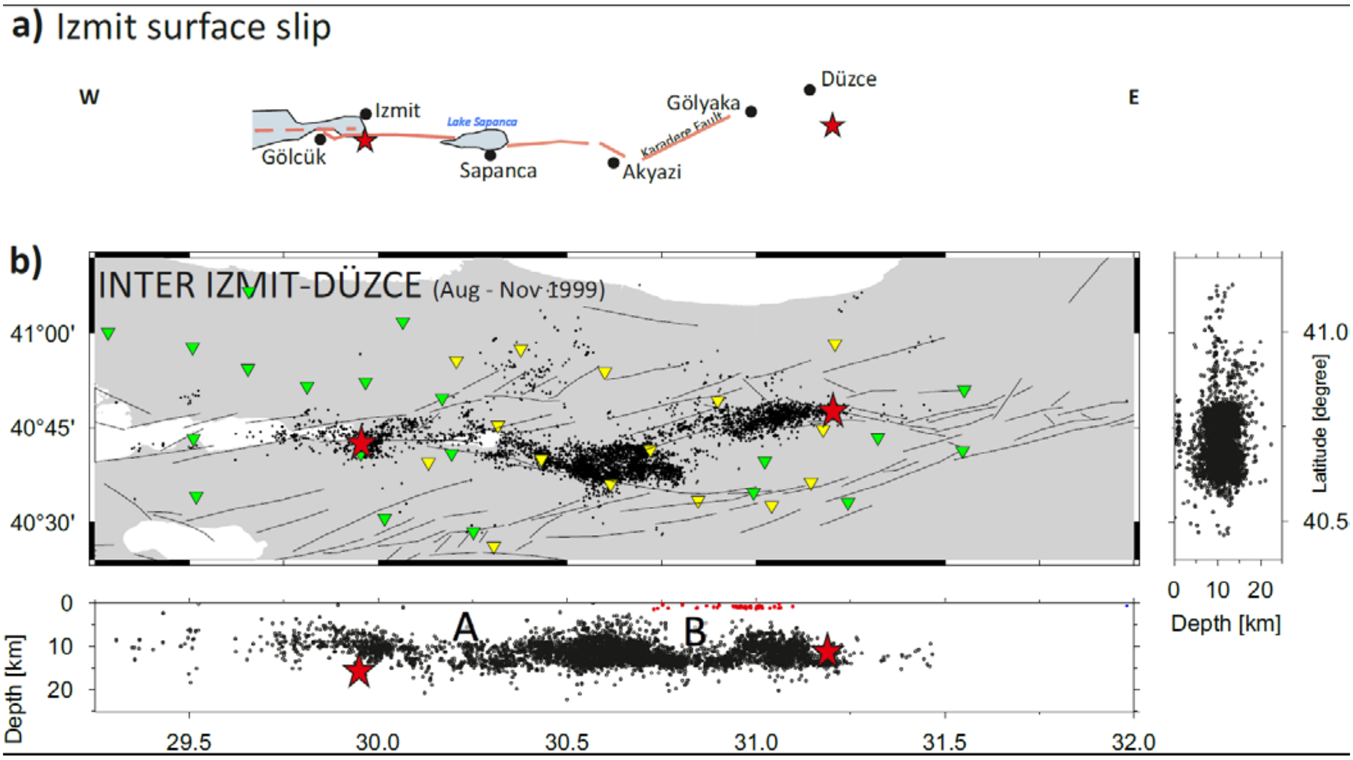

a) Izmit surface slip
W
E
Izmit
Gölcük
Lake Sapanca
Sapanca
Akyazi
Gölyaka
Karadere Fault
Düzce
b)
INTER IZMIT-DÜZCE (Aug - Nov 1999)
41°00'
40°45'
40°30'
41.0
40.5
Latitude [degree]
0 10 20
Depth [km]
A
B
0
10
20
Depth [km]
29.5
30.0
30.5
31.0
31.5
32.0

Figure 7

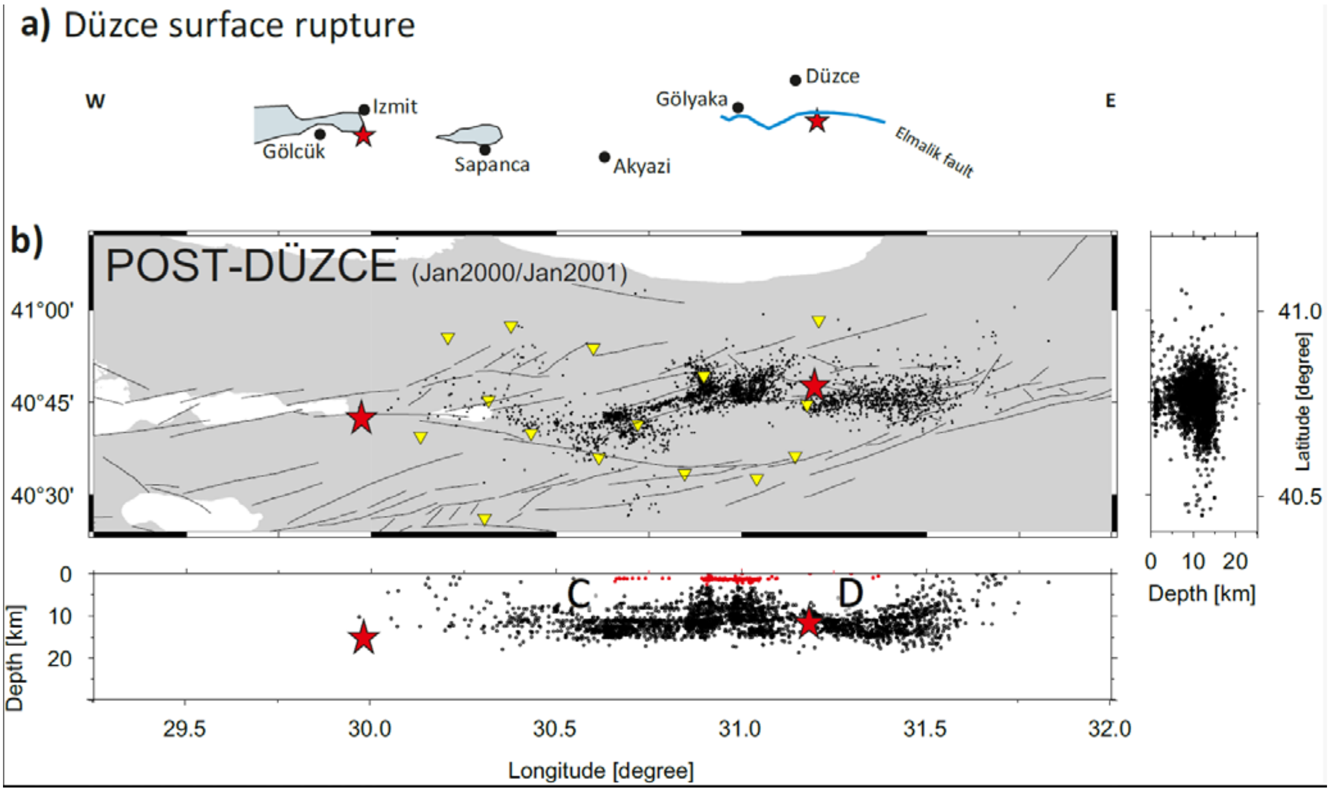

a) Düzce surface rupture
W
E
Izmit
Gölcük
Sapanca
Akyazi
Gölyaka
Düzce
Elmalik fault
b)
POST-DÜZCE (Jan2000/Jan2001)
41°00'
40°45'
40°30'
41.0
40.5
Latitude [degree]
0 10 20
Depth [km]
C
D
0
10
20
Depth [km]
29.5
30.0
30.5
31.0
31.5
32.0
Longitude [degree]

Figure 8

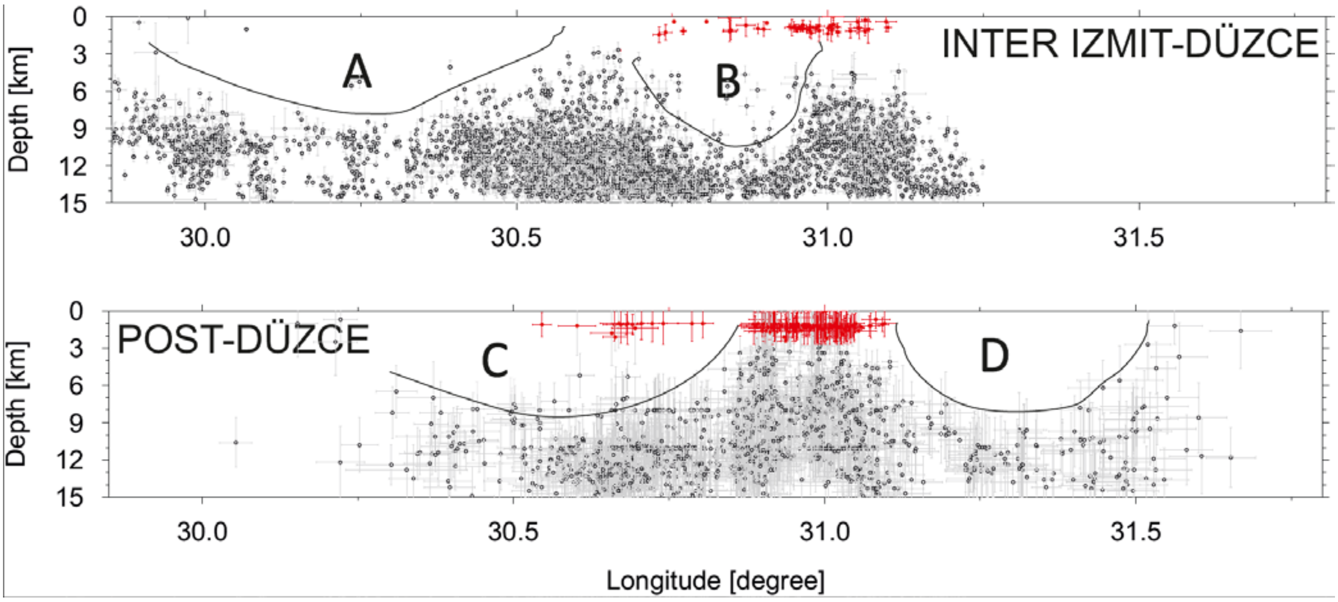
INTER IZMIT-DÜZCE
A
B
Depth [km]
0
3
6
9
12
15
30.0
30.5
31.0
31.5
POST-DÜZCE
C
D
Depth [km]
0
3
6
9
12
15
30.0
30.5
31.0
31.5
Longitude [degree]

Figure 9:

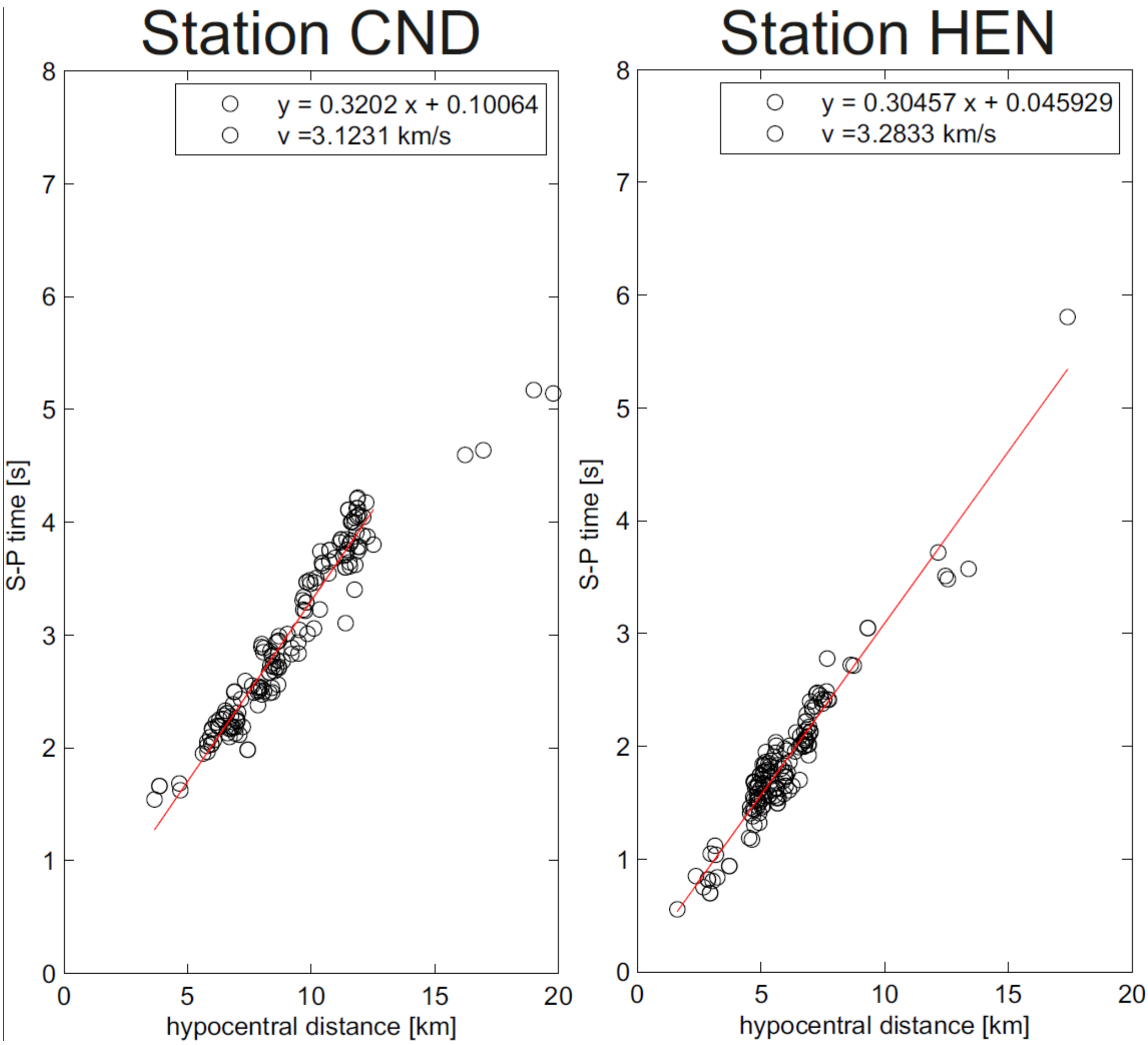

Station CND
y = 0.3202 x + 0.10064
v =3.1231 km/s
S-P time [s]
hypocentral distance [km]
Station HEN
y = 0.30457 x + 0.045929
v =3.2833 km/s
S-P time [s]
hypocentral distance [km]

Figure 10a:

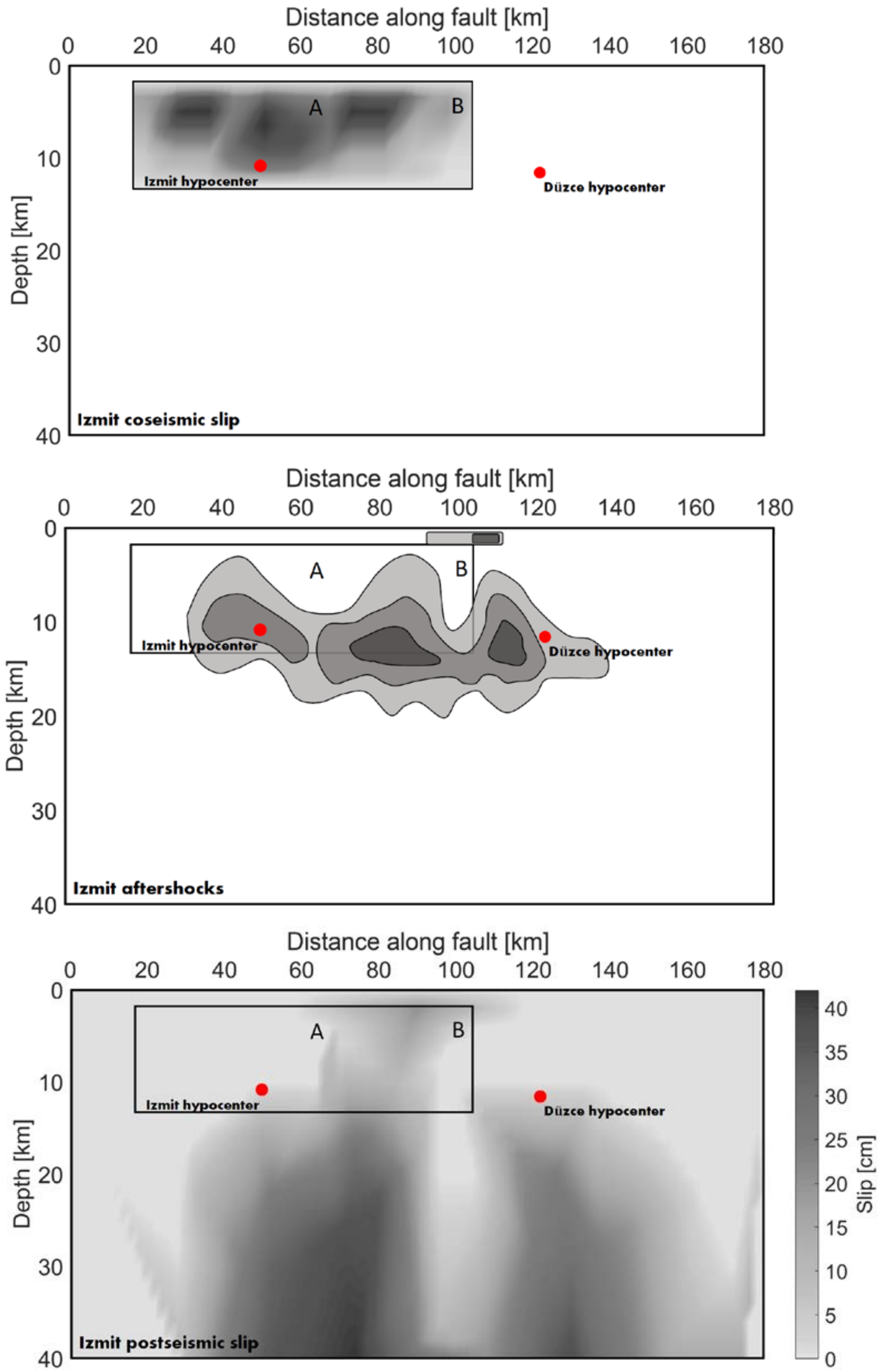

Distance along fault [km]
0
20
40
60
80
100
120
140
160
180
Depth [km]
0
10
20
30
40
A
B
Izmit hypocenter
Düzce hypocenter
Izmit coseismic slip
Distance along fault [km]
Depth [km]
A
B
Izmit hypocenter
Düzce hypocenter
Izmit aftershocks
Distance along fault [km]
Depth [km]
A
B
Izmit hypocenter
Düzce hypocenter
Izmit postseismic slip
Slip [cm]
40
35
30
25
20
15
10
5
0

Figure 10b:

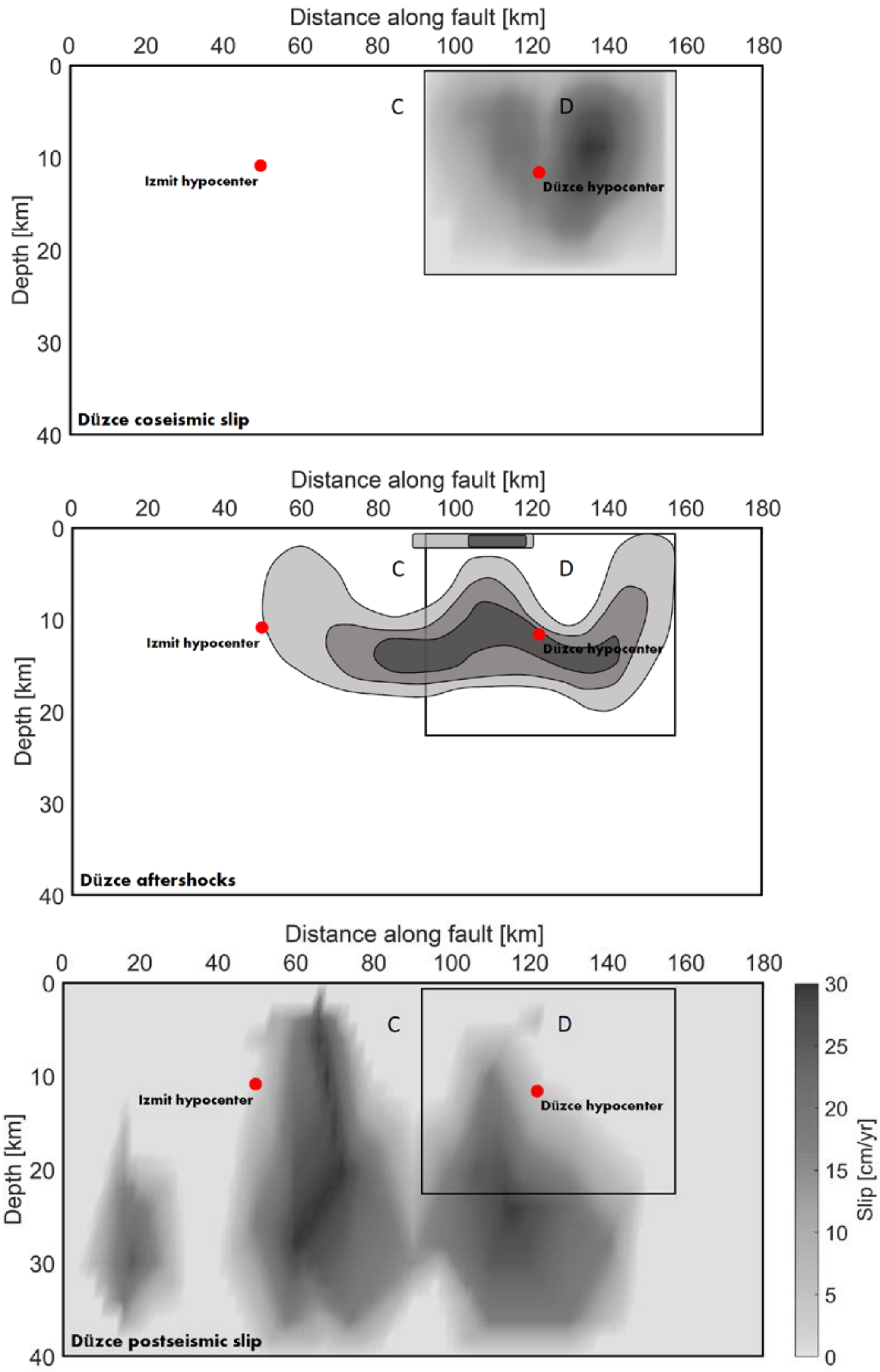

Distance along fault [km]
Depth [km]
C
D
Izmit hypocenter
Düzce hypocenter
Düzce coseismic slip
Düzce aftershocks
Düzce postseismic slip
Slip [cm/yr]

Figure 11:

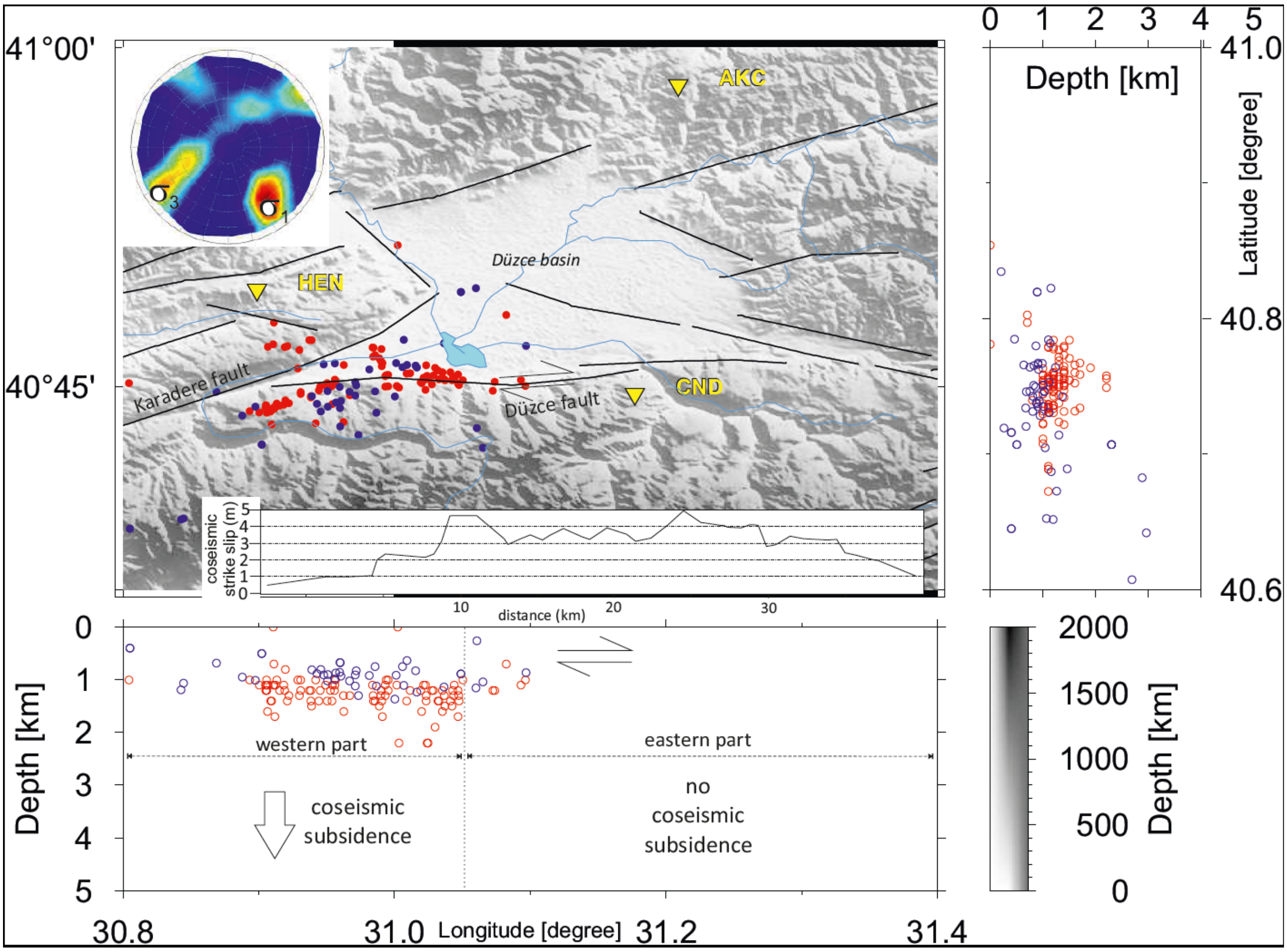

41°00'
40°45'
AKC
HEN
CND
Düzce basin
Karadere fault
Düzce fault
coseismic strike slip (m)
distance (km)
Depth [km]
Latitude [degree]
41.0
40.8
40.6
western part
eastern part
coseismic subsidence
no coseismic subsidence
Longitude [degree]
30.8
31.0
31.2
31.4
2000
1500
1000
500
0